

AFWAL-TR-84-3056



TEMPERATURE RESPONSES OF COMPOSITE PANELS

No DTIC

Lit S. Han
Department of Mechanical Engineering
The Ohio State University
Columbus, Ohio 43210-1365

September, 1984

Final Report for Period June 1983-May 1984

Approved for public release; distribution unlimited.

FLIGHT DYNAMICS LABORATORY
AIR FORCE WRIGHT AERONAUTICAL LABORATORIES
AIR FORCE SYSTEMS COMMAND
WRIGHT-PATTERSON AIR FORCE BASE, OHIO 45433

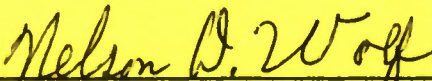
APA 150053

NOTICE

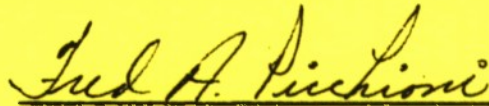
When Government drawings, specifications, or other data are used for any purpose other than in connection with a definitely related Government procurement operation, the United States Government thereby incurs no responsibility nor any obligation whatsoever; and the fact that the government may have formulated, furnished, or in any way supplied the said drawings, specifications, or other data, is not to be regarded by implication or otherwise as in any manner licensing the holder or any other person or corporation, or conveying any rights or permission to manufacture use, or sell any patented invention that may in any way be related thereto.

This report has been reviewed by the Office of Public Affairs (ASD/PA) and is releasable to the National Technical Information Service (NTIS). At NTIS, it will be available to the general public, including foreign nations.

This technical report has been reviewed and is approved for publication.



NELSON D. WOLF, Project Engineer
Design & Analysis Methods Group



FREDERICK A. PICCHIONI, Lt Col, USAF
Chief, Analysis & Optimization Branch

FOR THE COMMANDER



ROGER J. HEGSTROM, Colonel, USAF
Chief, Structures & Dynamics Div.

If your address has changed, if you wish to be removed from our mailing list, or if the addressee is no longer employed by your organization please notify AFWAL/FIBRA, W-PAFB, OH 45433 to help us maintain a current mailing list.

Copies of this report should not be returned unless return is required by security considerations, contractual obligations, or notice on a specific document.

REPORT DOCUMENTATION PAGE		READ INSTRUCTIONS BEFORE COMPLETING FORM
1. REPORT NUMBER AFWAL-TR-84-3056	2. GOVT ACCESSION NO.	3. RECIPIENT'S CATALOG NUMBER
4. TITLE (and Subtitle) TEMPERATURE RESPONSES OF COMPOSITE PANELS		5. TYPE OF REPORT & PERIOD COVERED Final; June, 1983-May, 1984
		6. PERFORMING ORG. REPORT NUMBER
7. AUTHOR(s) Dr. Lit S. Han		8. CONTRACT OR GRANT NUMBER(s) F33-615-83-C-3000
9. PERFORMING ORGANIZATION NAME AND ADDRESS Mechanical Engineering Department, The Ohio State University, 206 W. 18th Ave., Columbus, Ohio 43210		10. PROGRAM ELEMENT, PROJECT, TASK AREA & WORK UNIT NUMBERS P.E. 62201F 2401-02-44
11. CONTROLLING OFFICE NAME AND ADDRESS AFWAL/FIBRA WPAFB, OH, 45433		12. REPORT DATE September 1984
		13. NUMBER OF PAGES 85
14. MONITORING AGENCY NAME & ADDRESS (if different from Controlling Office)		15. SECURITY CLASS. (of this report) Unclassified
		15a. DECLASSIFICATION/DOWNGRADING SCHEDULE
16. DISTRIBUTION STATEMENT (of this Report) Approved for Public Release; Distribution Unlimited.		
17. DISTRIBUTION STATEMENT (of the abstract entered in Block 20, if different from Report)		
18. SUPPLEMENTARY NOTES		
19. KEY WORDS (Continue on reverse side if necessary and identify by block number) Composite Panels, Temperature Responses, Spot-Heating, Cyclic Heating		
20. ABSTRACT (Continue on reverse side if necessary and identify by block number) In this report, two transient heat conduction problems for application to the thermal evaluation of composite materials are analyzed and discussed. The purposes of these two analyses are at least two fold: One is to demonstrate by detailed numerical results that composite materials with a larger in-plane thermal conductivity than the transverse value exhibit lower surface temperatures when the thermal loading consists of irradiation by a concentrated cylindrical beam. Effective radial heat spread along the		

in-plane direction serves to reduce local heat accumulation and thereby mitigates heat-spot temperature rises. Accordingly, preventing or delaying damage due to high-intensity thermal radiation on composite surfaces can be enhanced by using materials with large in-plane thermal conductivities. The second objective of the investigation is to develop a methodology whereby composite panels undergoing cyclic heating and cooling can be analyzed for their periodic temperature responses. This is particularly important for determining thermal stresses resulting from alternating temperature fluctuations. The methodology developed is especially useful since numerical approaches can be very time-consuming and unreliable.

FOREWORD

With the increasing use of composites in aero-space structure components, survivability and vulnerability of the composites when exposed to intense thermal irradiation become a critical concern. New materials with desirable surface characteristics are being explored to mitigate the likely encountered thermal loadings; and parallel to these developments, more reliable methods of analyzing the effects of inspired surface heat flux on the interior temperature responses of composite structures are needed.

The investigation reported here is a preliminary step to examine the basic needs for analytic tools to assess the temperature distributions in composites. Contained in this report are a new method of analyzing cyclic surface temperature fluctuations, temperature response results of composite panels due to spot-heating, and a comparative study of the effect of surface coating on the temperature rise of a substrate layer.

The work was sponsored by Air Force Flight Dynamic Laboratory with Mr. Nelson Wolf as the Technical Monitor; it was begun in June 1983 and completed in May 1984.

TABLE OF CONTENTS

<u>Section</u>	<u>Page</u>
1 INTRODUCTION	1
2 AXIS-SYMMETRICAL SPOT-HEATING OF COMPOSITE SLABS	3
2.1 Analysis	3
2.2 Finite-Difference Solutions	7
2.3 Scope of Computations	13
2.4 Results and Discussion	14
2.5 Summary and Recommendations	30
3 TRANSIENT HEAT FLOW IN MULTI-LAYER COMPOSITES	37
3.1 Impulsive Surface Heat Flux	38
3.2 Cyclic Surface Temperature	49
3.3 Cyclic Surface Heat Flux	62
4 CONCLUSIONS	73
REFERENCES	78
NOMENCLATURE	79
APPENDIX	81

List of Figures

<u>Figure</u>		<u>Page</u>
1	Cylindrical Irradiation Beam Configuration	4
2	Node Definition	4
3	Heat Spot and Back Temperatures for Isotropic Conductivity, $k_r/k_z = 1$	16
4	Heat Spot Temperature Rises for Large In-Plane Thermal Conductivities, $w/a = 1$	17
5	Heat Spot and Back Temperature Rises by Thermal Shieldings, $k_r/k_z = 4$	18
6	Heat Spot and Back Temperature Rises by Thermal Shieldings, $k_r/k_z = 9$	19
7	Model of Constant Heating of an Infinite-Medium Internally Bounded by a Cylindrical Surface	25
8	Heat Spot Temperature Rises, all Cases	26
9	Asymptotic Variations of Heat Spot Temperature Rises	27
10	Spot Heating Isothermal Contours at Various Conductivity Ratios, $w/a = 1$	28
11	Spot Heating Isothermal Contours for $w/a = 4$ and $k_r/k_z = 1$	32
12	Spot Heating Isothermal Contours for $w/a = 4$ and $k_r/k_z = 9$	33
13	Surface Temperature Profiles at Various Conductivity Ratios, $w/a = 1$	34
14	Surface Temperature Profiles at Various Conductivity Ratios, $w/a = 4$	35
15	Two-Layer Composite Configuration and Definitions	42
16	Interface Temperature Rises Due to Constant Heat Flux at Various Coating Conductivities	46

List of Figures (continued)

<u>Figure</u>	<u>Title</u>	<u>Page</u>
17	Interface Temperature Rises Due to Constant Heat Flux at Various Coating Thermal Capacity Ratios	47
18	Back Surface Temperature Rises Due to Constant Heat Flux at Various Coating Thermal Capacity Ratios	48
19	Multi-Layer Panel Configuration and Definitions	53
20	Temperature Functions of a 4-Layered Composite Due to Periodic Surface Temperature Variation	64
21	Temperature Responses of a Single-Layer Composite by Periodic Surface Temperature Variation	65
22	Temperature Responses of a Two-Layer Composite by Periodic Surface Temperature Variation, $(\rho C)_c / (\rho C)_s = 4$	66
23	Temperature Responses of a Two-Layer Composite by Periodic Surface Variation, $k_c / k_s = 0.2$	67
24	Temperature Responses of a Two-Layer Composite by Periodic Surface Temperature Variation, $k_c / k_s = 0.1$	68
25	Temperature Responses of a Single-Layer Composite by Periodic Surface Heat Flux	75
26	Influence of Large Coating Layer Thermal Capacity on Temperature Responses of a Two-Layer Composite by Periodic Surface Heat Flux	76
27	Influence of Low Coating Layer Thermal Conductivity on Temperature Responses of a Two-Layer Composite by Periodic Surface Heat Flux	77
A-1	Effect of Grid Size on Temperature Calculations, Spot Heating	83
A-2	Effect of Grid Size on Isothermal Contours, Spot Heating	84
A-3	Effect of Grid Size on Surface Temperature Profiles, Spot Heating	85

1. INTRODUCTION

Light weight, high strength and dimensional stability are among the principal advantages of composite materials in comparison to metals, and consequently have led to their ever-increasing use in aerospace structures. For the same reasons, a lengthening list of new composite materials is emerging into the marketplace for specific applications. In the new applications there exist environmental factors, heretofore un contemplated, where thermal considerations are a prime concern. Severity of the thermal environments, in which composite materials are expected to function, plays a critical role not only in their selection, but also in the conceptual stage of composites' development as aerospace structural components. In order to assess the ability of composite materials from a thermal viewpoint, an analytical determination of the temperature responses of candidate structures is of course a first step leading to, and pinpointing, further refinements and subsequent developmental efforts.

For thermal analysis, the most fundamental characteristic of composite materials is the effective thermal conductivity; it is essentially reflective of the physical relationships between different phases of materials in a composite medium. In the case of a typical composite -- graphite fibers in an epoxy binding matrix -- the dispersion pattern, relative size, and density of fibers are the governing criteria that determine an effective conduction coefficient. Experimental effective thermal conductivities exist only for a very few composite materials,

and moreover, they are mostly for fabricated specimens of fixed compositions. These ad hoc data, scattered and scanty, are difficult to organize and to relate to one another in order to form engineering correlations; the situation is not unlike that of the newly developed aluminum alloys decades ago when industry-wide standards were still in their formative stages.

Coupled with the need for more reliable thermo-physical properties, consideration must be given to the types of analysis for examining thermal responses of composite materials in high-temperature environments. Instead of an overview of the entire spectrum of the heat conduction phenomena, a narrower but pragmatic perspective of survivability and vulnerability of composite materials in aerospace structure is adopted. From such a perspective, this report addresses two major problem areas which constitute two main critical tests for a composite material to survive; and they are undertaken in this report not as exhaustive accounts from an operational viewpoint, but as demonstrative studies for establishing the methodology of each. Results of the two case studies are discussed in terms of thermo-physical properties of the composites and their parametric relations with calculated temperature responses. From the calculated results, guidelines are established for an assessment of composites' ability to withstand the intended thermal environment.

The first problem concerns the localized thermal heating of a panel by a cylindrical beam of irradiation. As composite materials in general are characterized by orthotropical conductivities, the analysis focuses on the effect of the in-plane thermal conductivity upon the heat

penetration pattern. The second problem deals with the temperature response of a multi-layer composite subjected to cyclic surface heating, which is a representative encounter for an orbiting space vehicle. Both problems are limited to their parametric performances of temperature responses, and their subsequent physical phenomena -- melting or ablation in the first case and buckling with alternating thermal stresses in the second -- are not discussed in this report.

2. AXIS-SYMMETRICAL SPOT-HEATING OF COMPOSITE SLABS

Consider a slab with a thermal irradiation loading by a cylindrical beam of constant heat flux. The material of the slab is such that the thermal conductivity in the plane of the slab is isotropic but differs from the conductivity in the depth direction. Such a combination of thermal conductivities typifies composites with fibers oriented in the plane of the slab. Composites with fibers in overlay patterns of 0/90, 0/±45/90 all fall into this category.

The slab is initially at a uniform temperature, arbitrarily taken to be zero, and as spot-heating proceeds, the temperature rise of the panel is to be determined.

2.1 Analysis. Figure 1 depicts schematically the thermal system under consideration. Thermal irradiation is confined to a radius of a and is of intensity Q . Axis-symmetry is assumed and the heat diffusion equation together with its boundary conditions are:

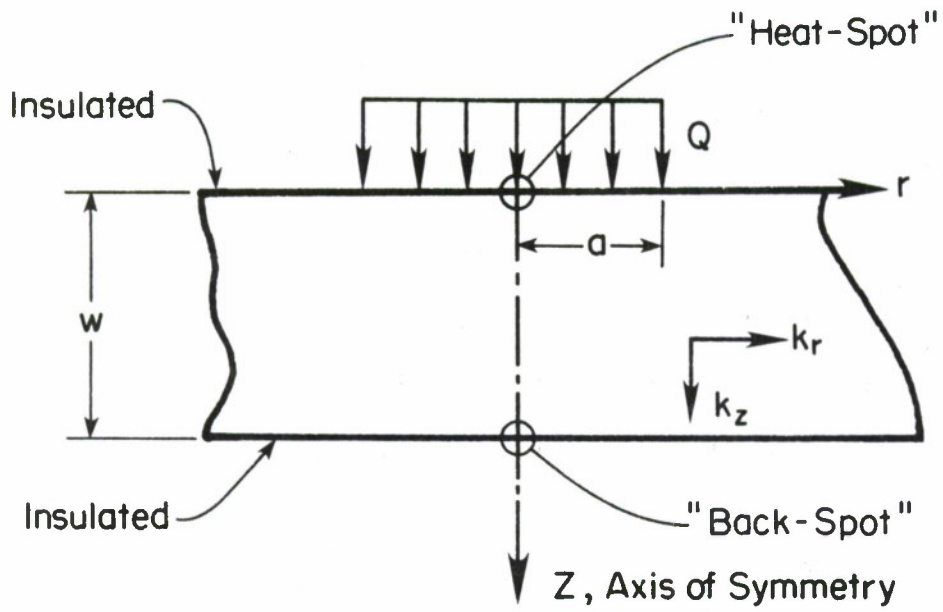


Figure 1. Cylindrical Irradiation Beam Configuration

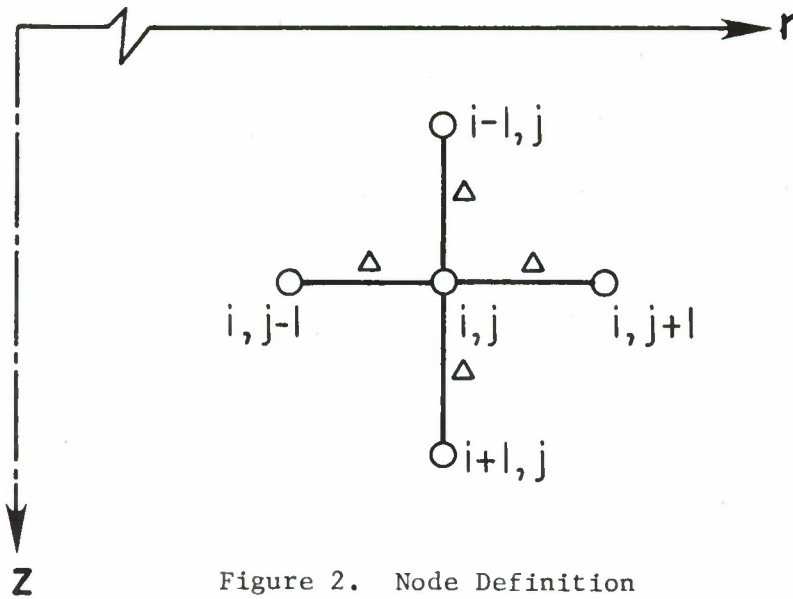


Figure 2. Node Definition

$$\rho C \frac{\partial T}{\partial \theta} = k_r \left(\frac{\partial^2 T}{\partial r^2} + \frac{1}{r} \frac{\partial T}{\partial r} \right) + k_z \frac{\partial^2 T}{\partial z^2} \quad (1)$$

$$-k \frac{\partial T}{\partial z} = Q \quad \text{at } z = 0, \quad r < a \quad (2)$$

$$\frac{\partial T}{\partial z} = 0 \quad \text{at } z = 0, \quad r > a; \text{ and at } z = w \quad (3)$$

Except at the irradiation beam, all surfaces are insulated and the slab is considered infinite in the in-plane direction. The characteristic parameters are a , w , Q and the thermal properties (ρC) , k_r , and k_z , all of which are needed to express the results in non-dimensional forms. The terms of the right-hand side of equation (1) represent of course the heat fluxes in the r and z -direction respectively, which lead to the following non-dimensional variables:

$$\bar{r} = (r/a) \sqrt{k_z/k_r} \quad (4)$$

$$\bar{z} = z/a \quad (5)$$

$$\bar{\theta} = (\alpha_z \theta / a^2) \quad (6)$$

where α_z is the thermal diffusivity and is given by

$$\alpha_z = k_z / (\rho C) \quad (7)$$

The preceding transformations, particularly equations (4) and (5), indicate a scale change in the r -direction because of different thermal conductivities k_r and k_z . By defining a non-dimensional temperature as

$$\bar{T} = \frac{Tk_z}{aQ} \quad (8)$$

the preceding equations are rendered non-dimensional as follows:

$$\frac{\partial \bar{T}}{\partial \bar{\theta}} = \frac{\partial^2 \bar{T}}{\partial \bar{r}^2} + \frac{1}{\bar{r}} \frac{\partial \bar{T}}{\partial \bar{r}} + \frac{\partial^2 \bar{T}}{\partial \bar{z}^2} \quad (9)$$

The boundary conditions become

$$\frac{\partial \bar{T}}{\partial \bar{z}} = -1 \quad \bar{z} = 0, \bar{r} < \sqrt{k_z/k_r} \quad (10)$$

$$\frac{\partial \bar{T}}{\partial \bar{z}} = 0 \quad \bar{z} = 0, \bar{r} > \sqrt{k_z/k_r} \quad (11)$$

$$\frac{\partial \bar{T}}{\partial \bar{z}} = 0 \quad \bar{z} = w/a \quad (12)$$

Initially, before heat flux at $z = 0$, the temperature is zero, or

$$\bar{T} = 0 \quad \bar{\theta} = 0 \quad (13)$$

The different scale changes in the r and z directions are made necessary because of different thermal conductivities in these two directions. Solution of the preceding set of equations can, in principle, be obtained by a rigorous, exact approach, for example, by a Laplace transform in θ , a Fourier transform in z and a Hankel transform in r . Such

an approach is conceptually satisfying; however, the inversion procedures necessary for computation may become so involved that the method is itself rendered impractical and moot. Hence, in order to produce numerical results for making engineering judgements, the finite-difference approach is used and its implementation is described next.

2.2 The Finite-Difference Solution. For diffusion problems, the simplest scheme is a combination of three-point central difference in space and one time-step marching using explicit algebra. It however suffers from the disadvantage of being unstable which can only be cured by using smaller time steps. Implicit schemes are known to be unconditionally stable but requires the inversion of large matrixes. In one-dimensional problems, the matrixes are tri-diagonal; but in multi-dimensional ones, the matrixes are not so simple. And so far, no simple algorithms have been devised.

Instead of the fully implicit and fully explicit method, a viable choice is the alternating-direction explicit method [1] which has a greater degree of stability and is therefore less time consuming than the explicit method. In addition, the necessary algebraic manipulation is much less involved than the implicit method, especially for multi-dimensional problems.

Since the heat beam radius is a governing dimension of the problem, the size of a finite-difference grid begins at the heat spot. Along its

radius, 5^* divisions are used. The exact numerical value of $\Delta \bar{r}$ is dependent, of course, on the relative magnitudes of k_r and k_z . By definition $\bar{r} = (r/a)\sqrt{k_z/k_r}$, hence from $r = 0$ to $r = a$ there are five equal increments, each equal to $\Delta \bar{r} = 0.2\sqrt{k_z/k_r}$, with the ratio of the two conductivity values varying from one problem specification to another. To attain equal accuracy in the z -direction, equation (9) requires that $\Delta \bar{z} = \Delta \bar{r}$. In this way the mesh size is made flexible, depending on the relative magnitudes of the conductivities. The total number of nodes in the \bar{z} -direction is determined by the slab thickness (w/a).

It should be mentioned that in the finite-difference algorithm used for the two-dimensional problems, a single-indexed temperature array is used. Customarily, a double-indexed array is for keeping track of the nodal positions. However, owing to the undetermined numbers of nodes in both directions, single-indexed arrays are better suited to the situation; the node positions can be easily identified by the array index in question. For example, if there are 20 nodes in \bar{z} and 500 in \bar{r} , a single array of variables with index from 1 to 10000 is needed. The same array can also be used for 500 nodes in \bar{z} and 20 in \bar{r} . A simple accounting of the index value serves to identify the node in question.

In presenting the various finite-difference formulas, however, the usual two-index notations are used for simplicity and ease of discussion.

* The effects of using 10 divisions are documented in Appendix A

The Finite-Difference Formula for Regular Nodes. A node located in the interior of the slab but not the axis of symmetry is termed regular node. Using two-indexed notations, $T_{i,j}$ is the temperature at the node position identified by the two indexes. On the exposed surface where heating occurs, $i = 1$ and on the axis of symmetry, $j = 1$; nodes on these locations are not regular nodes. The finite-difference formula for regular nodes is based on a r - z mesh of equal increments as are for other nodes. A five-point cluster of nodes is illustrated in Figure 2 together with their definitions.

According to the ADE method, the second-order derivative on the right of equation (9) is replaced by a time-splitting procedure. Thus

$$\frac{\partial^2 \bar{T}}{\partial r^2} = \left[(T_{i,j+1} - T_{i,j}) - (T_{i,j}^n - T_{i,j-1}^n) \right] / \Delta^2 \quad (14)$$

Superscript n denotes the nodal values at a later time step, or "new" values; otherwise, current values are meant. The same increment of $\Delta \bar{r}$ and $\Delta \bar{z}$ is denoted by a common symbol Δ . Similarly, the following is also valid:

$$\frac{\partial^2 \bar{T}}{\partial z^2} = \left[(T_{i+1,j} - T_{i,j}) - (T_{i,j}^n - T_{i-1,j}^n) \right] / \Delta^2 \quad (15)$$

The first-order derivative of equation (9) is given by a central-difference approximation, again using split-time values,

$$\frac{\partial \bar{T}}{\partial r} = (T_{i,j+1} - T_{i,j-1}^n) / (2\Delta) \quad (16)$$

$$\frac{\partial \bar{T}}{\partial \theta} = (T_{i,j}^n - T_{i,j}) / \delta \quad (17)$$

where δ represents the time step $\delta = \Delta\theta$. Incorporating these individual expressions into equation (9), the resulting formula for the calculation of $T_{i,j}^n$ is given by

$$\begin{aligned} T_{i,j}^n = & \left\{ (\delta/\Delta^2) [T_{i,j+1} + T_{i+1,j} + T_{i,j-1}^n + T_{i-1,j}^n] \right. \\ & \left. + (\delta/\Delta^2) [T_{i,j+1} - T_{i,j-1}^n] / \bar{r} + T_{i,j} [1 - 2(\delta/\Delta^2)] \right\} \\ & / [1 + 2(\delta/\Delta^2)] \end{aligned} \quad (18)$$

Elementary considerations of the stability question lead to a positive coefficient of $T_{i,j}$ on the right of equation (18). Thus the time step δ is related to the space step Δ by

$$\delta < (\Delta^2/2) \quad (19)$$

In fact, as shall be developed later, the time step δ is taken to be

$$\delta = \Delta^2/2 \quad (20)$$

Even though the right-hand side of equation (18) contains nodal values at a new time, these are already known from the preceding calculations if the finite-difference computations are proceeding in the direction of increasing index numbers.

The Finite-Difference Formula for Central Nodes ($\bar{r} = 0$). For the nodes located on the axis of symmetry, where $\bar{r} = 0$, equation (18) is not valid since it contains a factor of $1/r$ on its right-hand side. The axis-symmetrical nature of the temperature distribution can be represented by an algebraic expression,

$$T = T_1 + b\bar{r}^2 \quad (21)$$

which satisfies the requirement $\partial T / \partial r = 0$ at $r = 0$. The temperature at $\bar{r} = 0$ is denoted by T_1 ; at $\bar{r} = \Delta$, the temperature denoted by T_2 is related to the coefficient b in equation (21). Equation (21) then becomes

$$T = T_1 + (T_2 - T_1)(\bar{r}^2 / \Delta^2) \quad (22)$$

which is valid for small values of \bar{r} . The r -derivatives of equation (9) can then be obtained from equation (22) and they become

$$\frac{\partial^2 \bar{T}}{\partial \bar{r}^2} = 2(T_2 - T_1) / \Delta^2 \quad (23)$$

$$\frac{1}{\bar{r}} \frac{\partial^2 T}{\partial \bar{r}} = 2(T_2 - T_1) / \Delta^2 \quad (24)$$

Expressed in terms of two-indexed notations and using the split-time schedule, the sum of these two terms is given by

$$\frac{\partial^2 \bar{T}}{\partial z^2} + \frac{1}{r} \frac{\partial \bar{T}}{\partial r} = 4(T_{i,2} - T_{i,1})/\Delta^2 \quad (25)$$

For the \bar{z} -direction, the split-time scheme results in

$$\frac{\partial^2 \bar{T}}{\partial z^2} = [T_{i+1,1} - T_{i,1} - (T_{i,1}^n - T_{i-1,1}^n)]/\Delta^2 \quad (26)$$

From equations (25) and (26), the finite-difference formula for central nodes is

$$T_{i,1}^n = \frac{[(\delta/\Delta^2)[T_{i+1,1} + T_{i-1,1}^n + 4T_{i,2}] + T_{i,1}[1 - (\delta/\Delta^2)]]}{[1 + 5(\delta/\Delta^2)]} \quad (27)$$

Stability considerations of equation (27) in calculating the new temperature lead to the criterion

$$\delta < \Delta^2 \quad (28)$$

which makes the coefficient of $T_{i,1}$ of equation (27) positive.

The criteria of equations (19) and (28) are both required and obviously the former is more stringent; hence the time step δ is governed by that of equation (20).

The Finite-Difference Formula for Boundary Nodes. The boundary condition at the slab top, $\bar{z} = 0$, is described through the first derivatives of the temperature by equation (10). Starting from the top

surface, the z-index is $i = 1, 2$, etc. The first derivative by a 3-point formula is therefore

$$\frac{\partial \bar{T}}{\partial z} = (4 T_{2,j} - T_{3,j} - 3T_{1,j})/2\Delta \quad (29)$$

For nodes located in the heating beam, $r < a$, equation (10) governs which raises the surface temperature $T_{i,j}$ to a new high value in successive time steps. By setting the derivative of equation (29) at -1 and replacing $T_{1,j}$ by $T_{1,j}^n$, a finite-difference formula for the new temperature is then established:

$$T_{1,j}^n = (4 T_{2,j} - T_{3,j} + 2\Delta)/3 \quad (30)$$

For nodes lying outside the irradiation beam, the condition of zero heat transfer results in

$$T_{1,j}^n = (4 T_{2,j} - T_{3,j})/3 \quad (31)$$

2.3 Scope of Computations

As this investigation is intended to exemplify and demonstrate the need of major areas of further research and to establish principal thermal criteria for composite application in aero-space structure, computational efforts were limited to the variations of a few major parameters so that conclusions can be drawn to pinpoint the future development of composite materials from a thermal protection viewpoint.

Accordingly, starting with the reference case of a panel with isotropic conductivity, i.e. $k_z = k_r$, two additional conductivity variations were analyzed: they are (i) radial (in-plane) thermal conductivity four times as large as the transverse value, $k_r = 4k_z$, and (ii) $k_r = 9k_z$ as the extreme case. Altogether, the conductivity ratios are 1, 4, and 9; these are considered adequate or at least representative of the expected variation.

Another geometrical parameter is the ratio of the panel thickness w to the spot radius a . In the computational effort of this analysis, values of (w/a) of 1, 2, and 4 were taken. Hence altogether, there are nine combinations of conductivity ratios and panel thickness ratios. From these combinations of the parameters, computed temperature responses due to impulsive spot heating are examined to formulate performance criteria for composite materials serving as thermal barriers to surface irradiation.

From a survivability and vulnerability standpoint, the criteria are temperature rise of the heating spot as heating proceeds, depth of heat penetration into the substrate, and back surface temperature rise. The temperature rises in conjunction with other relevant considerations -- such as glass/transition temperature or melting temperature, localized buckling and de-lamination, -- form the basis of selection and application of composite materials.

2.4 Results and Discussion

Spot-Surface Temperature Rise. The temperature rise at the center of the irradiation beam is the most important parameter of the thermal

response for judging how well a composite material endures a severe environment. In general terms, high temperature as a result of external thermal loads engenders various damages which may lead to progress incapacitation of the aerospace structures: possible damages include localized melting; structural buckling and fracture; layer delamination and crack initiative or enlargement; and, of course, thermal puncture due to mass removal. Multitude of these damage mechanisms precludes a complete analysis of each; instead, emphasis is placed on the role of the in-plane thermal conductivity in affecting the temperature response due to a confined irradiation beam.

Starting with the reference case of isotropic conductivity, i.e., $k_r = k_z$ and for panels with thickness ratios of $w/a = 1, 2$, and 4 , the spot center temperature rises are shown in Figure 3. The back surface temperature rises are also indicated. The frontal spot surface temperatures are identified by "s" and the back center spot temperatures by "b" in Figure 3 with the numerals preceding s or b indicating the slab thickness ratio.

An obvious trend of the temperature curves is that the magnitudes are mitigated by increased thickness from curve nos. 1s, 2s, to 4s; temperature reduction is more pronounced for the back surface temperature. These numerical values establish a reference with which other calculations can be compared. The reference performances in Figure 3 also illustrate the thermal protection available by straightforward thickening of thermal shields; in this case the additional panelty to reduce the front and back surface temperature rise is in direct proportion to the added thickness.

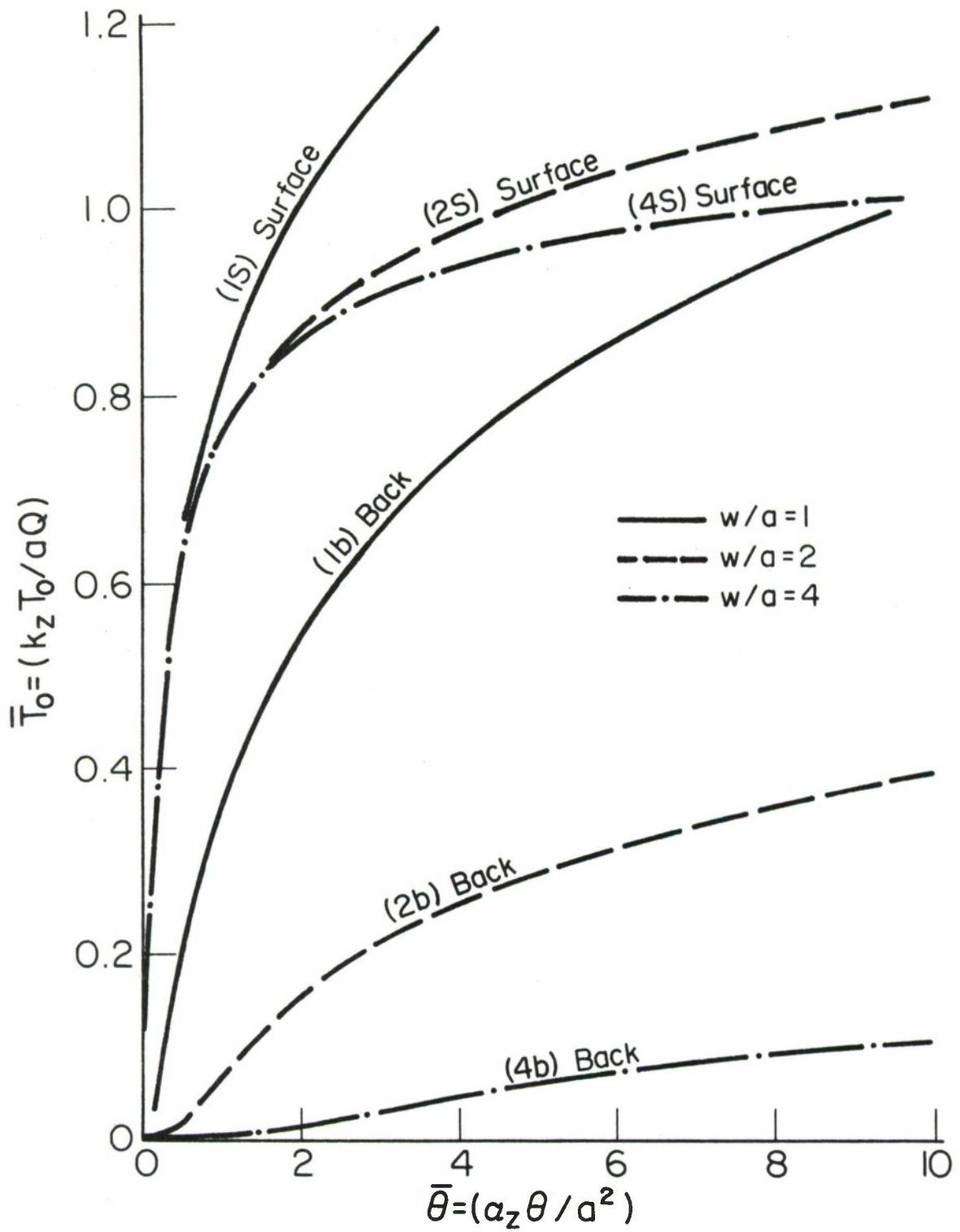


Figure 3. Heat Spot and Back Temperatures for Isotropic Conductivity, $k_r/k_z = 1$

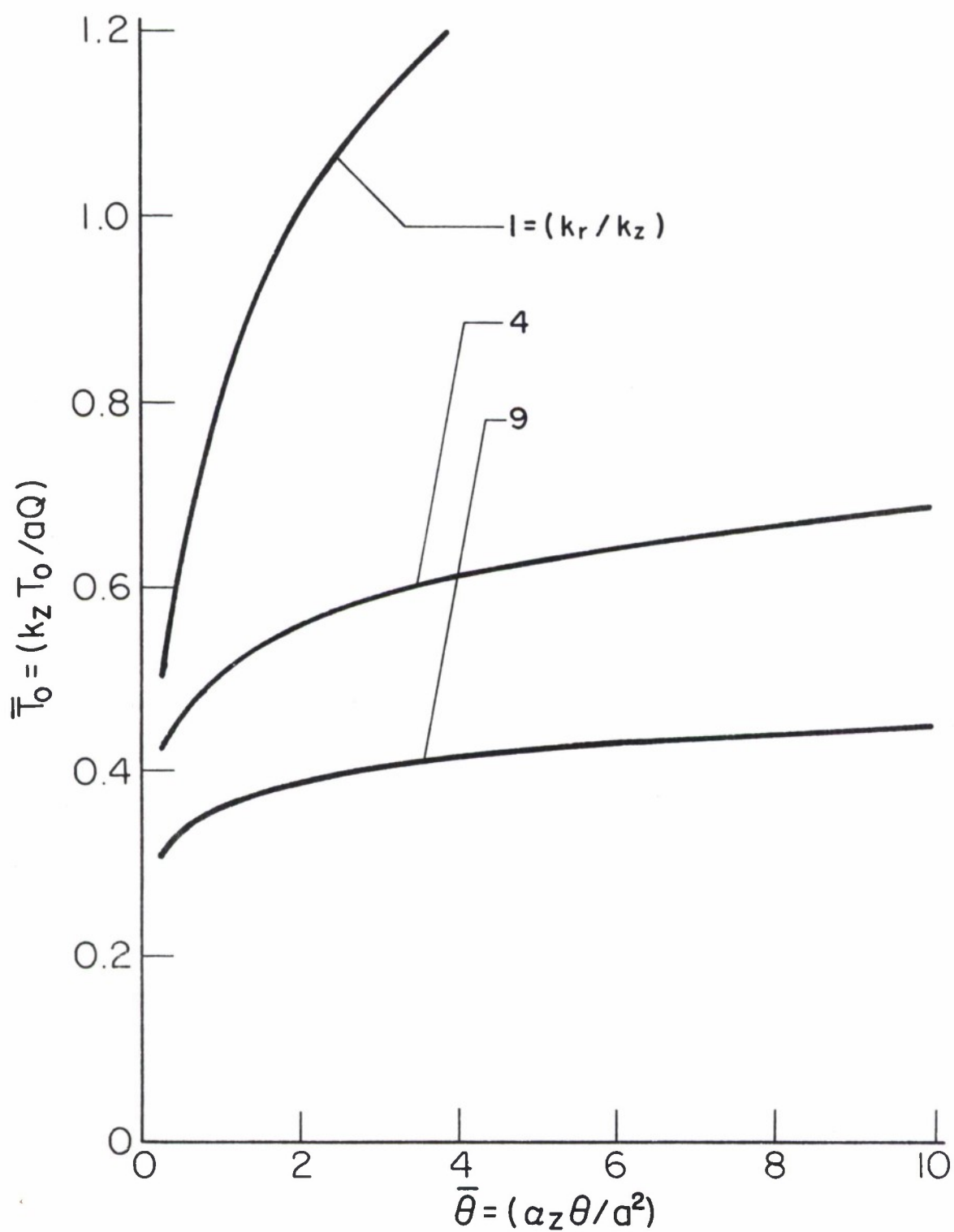


Figure 4. Heat Spot Temperature Rises for Large In-Plane Thermal Conductivities, $w/a = 1$

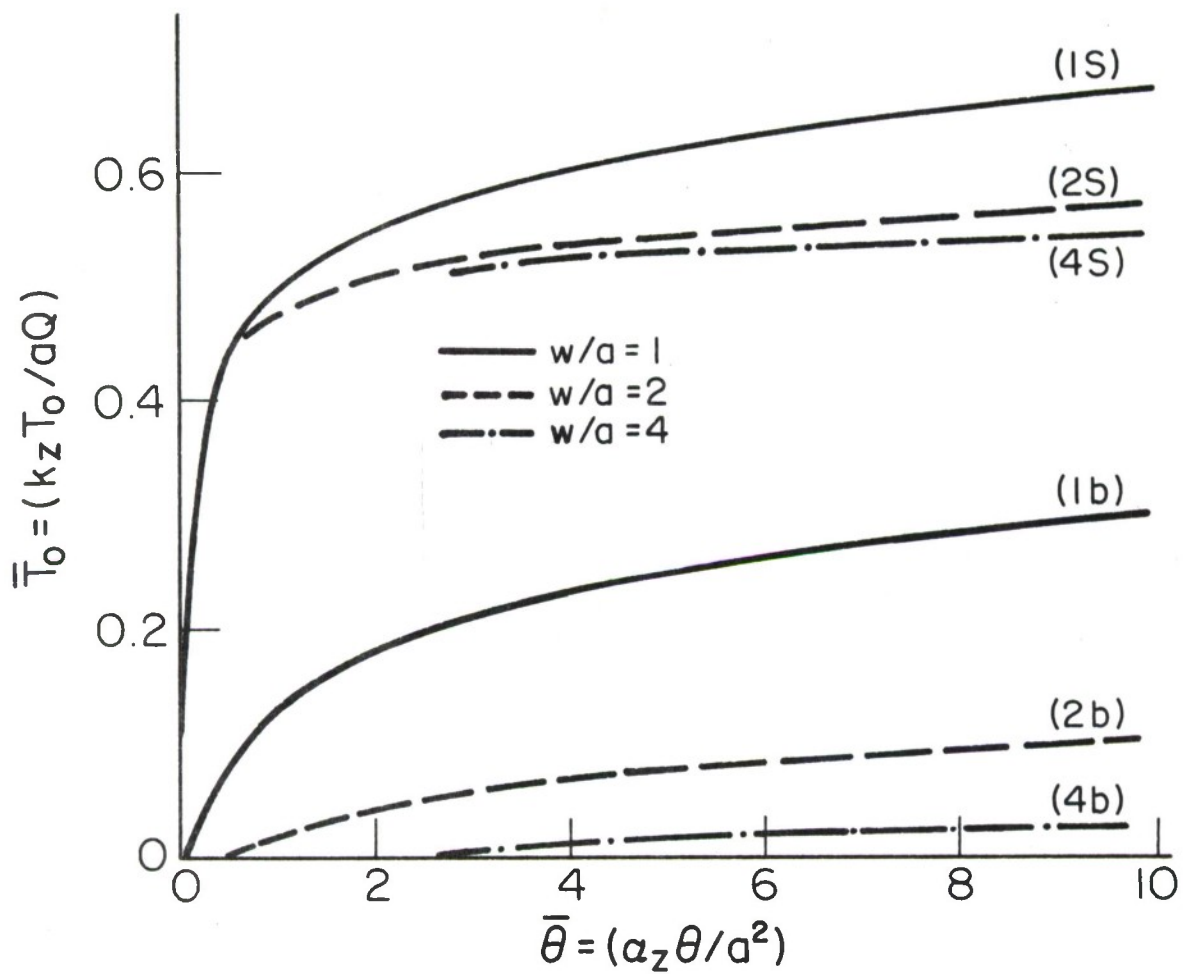


Figure 5. Heat Spot and Back Temperature Rises by Thermal Shieldings, $k_r/k_z = 4$

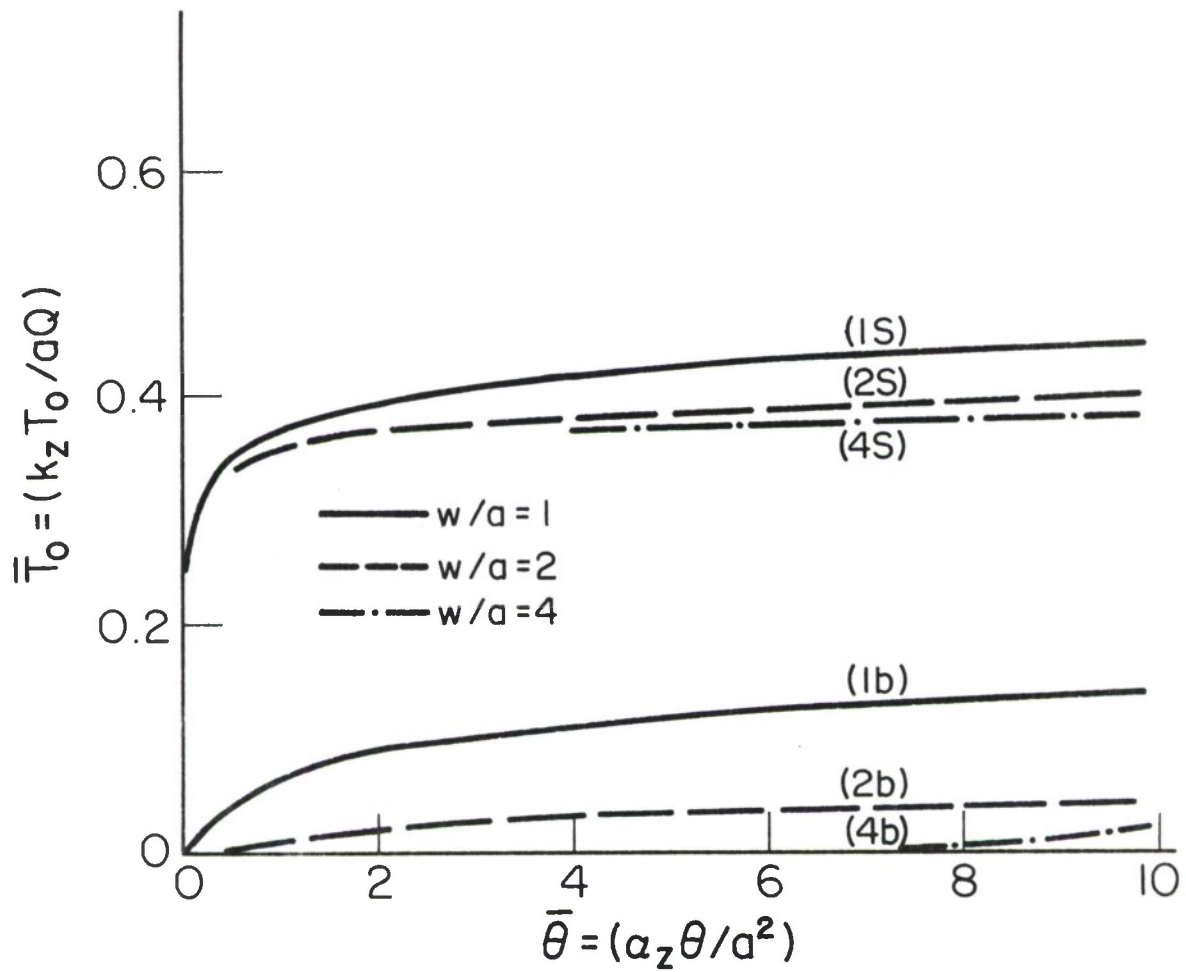


Figure 6. Heat Spot and Back Temperature Rises by Thermal Shieldings, $k_r/k_z = 9$

It is significant to note that as heating proceeds, the front surface and the back surface temperatures tend toward a fixed differential. Pairs of curves, for example, 1s, and 1b, gradually become parallel to each other. This phenomenon indicates that within the slab, the net heat flow occurs in the radial direction and is essentially spreading along the slab plane. In the early part of the heating period, say $\bar{\theta} < 1$, the heat spot temperature rises are similar to those of an infinite half-space with an impulsive surface heat flux. As heating proceeds, radial heat spread becomes effective and ultimately dominant in limiting the temperature change, as evidenced by the bending of the temperature curves.

This observation of the temperature trends lends itself to the interpretation, and indeed, expectation, that composite panels with large in-plane thermal conductivities would promote rapid lateral temperature spread and thereby reduce the front and back surface temperature rises.

To assess quantitatively the effect of large in-plane conductivity, additional computations are undertaken.

For a slab with a thickness ratio of $w/a = 1$ and conductivity ratios of $k_r/k_z = 1, 4$, and 9 , the computed temperature responses are grouped together in Figure 4. It is readily apparent that the temperature curves for $k_r/k_z = 4$ and 9 show very early trends toward the phenomenon of asymptotic radial heat flow from the heat source of the irradiation beam. The surface spot temperature rises are thus very much reduced compared to the case of $k_r/k_z = 1$; moreover, the temperature-rise limiting feature by virtue of the higher in-plane conductivity is more

effective than simple thickening of the thermal shield of an isotropic material, as shown in Figure 3.

To further bring out the relative performances, Figure 5 groups together the temperature calculations for $k_r/k_z = 4$ and slabs of thickness ratio of 1, 2 and 4. Figure 5 is a parallel to Figure 3; the latter is for $k_r/k_z = 1$. Similarly, Figure 6 contains the temperature data for $k_r/k_z = 9$ and the three thickness ratios. The performance data in these two figures demonstrate that large in-plane conductivities lead to an early (in time) asymptotic heat flow pattern of radial spread, thus reducing the front and back surface temperature rises. Further reductions of the temperatures are possible with additional thermal shield thickening, but the return is diminishing for higher ratios of k_r/k_z .

Asymptotic Trend of Temperature Variations. As shown by the preceding discussion, the heat spot temperature increases at first according to that of a semi-infinite medium with an impulsive heat flux across the entire surface. After a short time interval, the finite width of the slab and the limited heat beam radius begin to affect the temperature rise pattern: The pattern eventually becomes heat conduction in a finite-thickness sheet with heat input on the internal boundary of a cylindrical surface. Such an asymptotic configuration is defined in Figure 7, showing an internal boundary of radius a equal to the heat-beam radius and a heat flux magnitude q_r .

Such a heat flow problem has been analyzed and presented in [2]. For large times, the temperature rise at the heating boundary $r = a$ is given by

$$\frac{2k_r T_a}{aq_r} = \text{Log}_e [4(\alpha_r \bar{\theta}/a^2)] - 0.577 \quad (32)$$

A significant conclusion of equation (32) is that at large times, the temperature rise varies according to the log of time $\bar{\theta}$. To test such a correlation, the temperature rises computed for all nine cases are grouped together and plotted vs. the log of the lapse time $\bar{\theta}$.

Since the principal variable in the case studies is the in-plane thermal conductivity k_r , and the non-dimensional temperature and time use k_z and α_z as reference quantities in the ordinate and abscissa of Figure 8, in this way the relative magnitudes of \bar{T} give a direct indication of the surface heat spot temperatures.

To aid identification, these nine performance curves are numbered. The first set, nos. 1, 2, and 3, shows the temperature-time histories for the three slab thicknesses $w/a = 1, 2$ and 4 , and $k_r/k_z = 1$; the next set, nos. 4, 5, and 6, is for $k_r/k_z = 4$ and the same thickness variations; and the last set, nos. 7, 8, and 9, for $k_r/k_z = 9$. Having all nine cases together in a single graph again demonstrates the alleviation of the heat spot temperature rise by virtue of higher in-plane thermal conductivities, as contrasted to simple thicker thermal shields. More important is the feature that for longer heating time $\bar{\theta} > 4$, the semi-logarithmic plot in Figure 8 displays linear relations, thus essentially confirming the trend implicit in equation (32). The fact that for each case shown in Figure 8, the slope of its asymptotic variation is different from the others can be reconciled by noting the left-hand side of equation (32) and the non-dimensional ordinate of Figure 8. Equation (32) contains a radial heat flux q_r , as is indicated in Figure 7,

which is related to the surface heat flux Q in the irradiation beam by the following equivalence:

$$\pi a^2 Q = 2 \pi a w q_r$$

If q_r is eliminated from equation (32) by using the above relation, equation (32) is converted to

$$(w k_r T_a / a^2 Q) = 0.25 \log_e (\alpha_z \theta / a^2) + \text{constant} \quad (33)$$

where T_a denotes the temperature of the slab at the beam edge $r = a$. The re-organized temperature parameter on the left-hand side of equation (33) is then used to correlate the calculated temperature rise at the heat spot center -- but not the beam edge. The resulting relations for the nine cases are shown in Figure 9, where a prominent feature is that the asymptotic slopes for these curves are nearly equal to 0.30, which results in an equation of the form,

$$(w k_r T_o / a^2 Q) = 0.30 \log_e (\alpha_z \theta / a^2) + \text{constant} \quad (34)$$

where T_o is the heat spot center temperature.

Equations (33) and (34) differ from each other in the coefficients of 0.25 and 0.30, which are attributable to the different locations in the asymptotic equivalent configuration of Figure 7, where heating occurs at $r = a$ and in Figure 9, where T_o at $r = 0$ is used. Examination of the temperature profiles for the nine case studies indicates that there is a decline of the distribution from $r = 0$ to $r = a$ with a ratio

of $T_o/T_a = 1.25$; in other words, if T_a is used in lieu of T_o in Figure 9, the resulting slope would become $0.30/1.25 = 0.24$, which is in excellent agreement with the asymptotic radial heat spread requirement.

It should be emphasized that the matching of the asymptotic slopes with the simplified configuration of Figure 7 is not complete, for Figure 9 indicates that these variations still differ from one another by a constant term in equation (34); i.e., the curves are at different levels. This must be attributed to the different combinations of (k_r/k_z) and (w/a) in the finite-difference calculations; each one has a different temperature vs. time history in terms of heat storage, etc. before reaching their respective asymptotic states.

A factor of significance is that if the temperature response of a composite panel is to be analyzed, calculations can be terminated at a time asymptotic radial heat spread becomes established, after which time a semi-logarithmic formula can be used for extrapolating the spot surface temperature to larger values for $\bar{\theta}$.

Isotherms and Heat Penetration Depths. To further delineate the effect of the in-plane thermal conductivity, lines of constant temperature extracted from the numerical results are presented. Since there are a number of parametric variations in the cases analyzed, isothermal contours at $\bar{\theta} = 10$ only are considered. The isotherms are identified in terms of fractions of the heat spot surface temperature; this representation is necessary, for the individual temperatures of the heat spot surfaces are all different from each other.

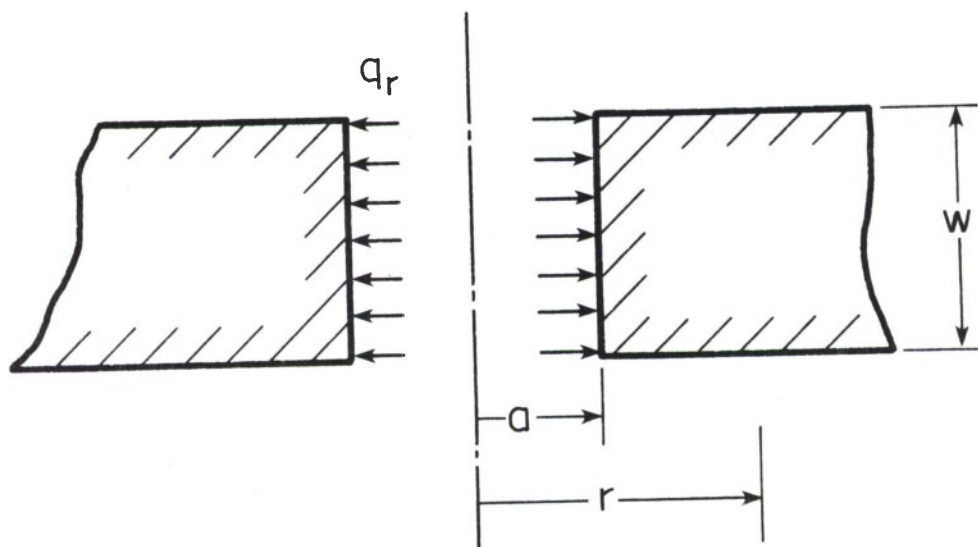


Figure 7. Model of Constant Heating of an Infinite Medium Internally Bounded by a Cylindrical Surface

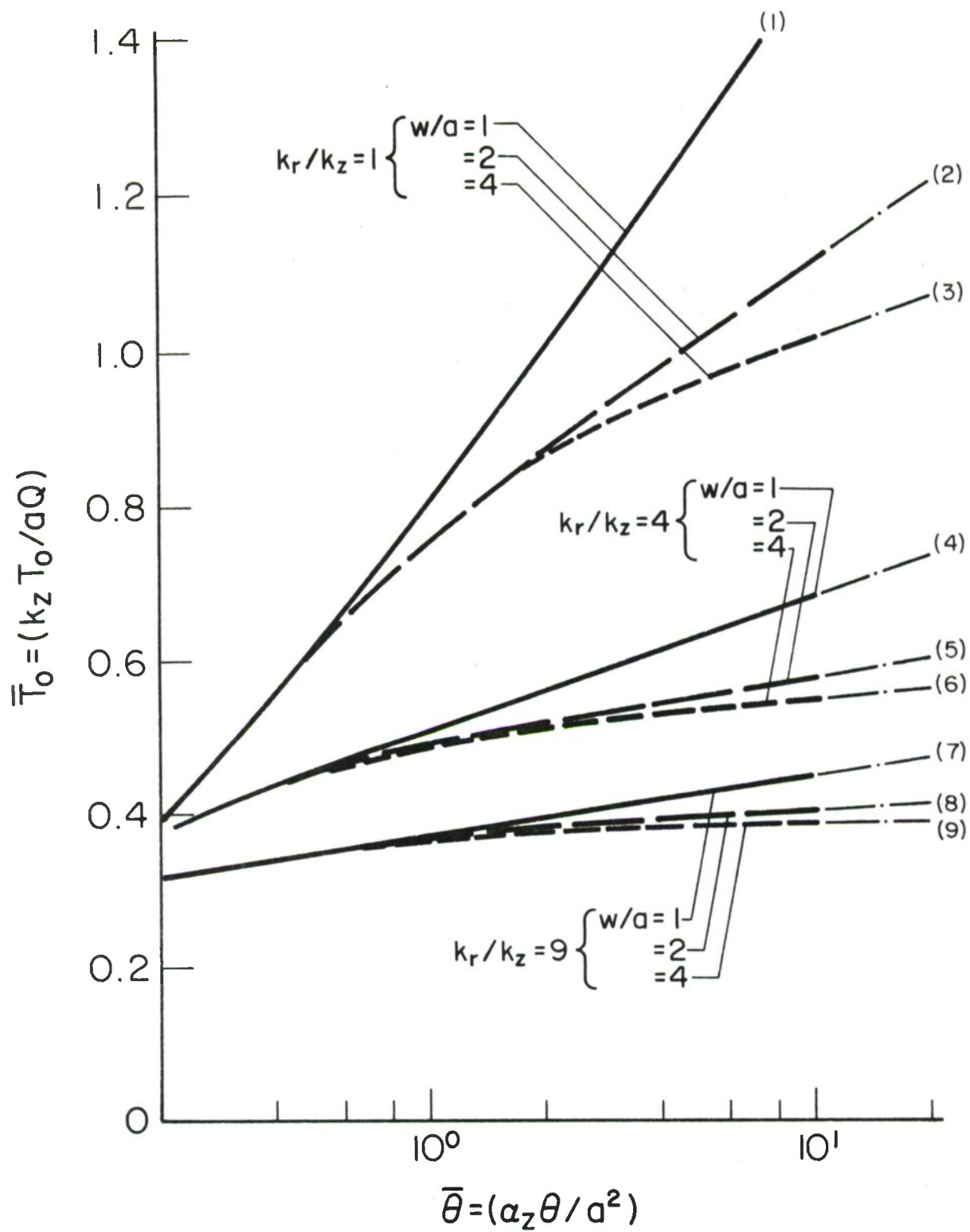


Figure 8. Heat Spot Temperature Rises, all Cases

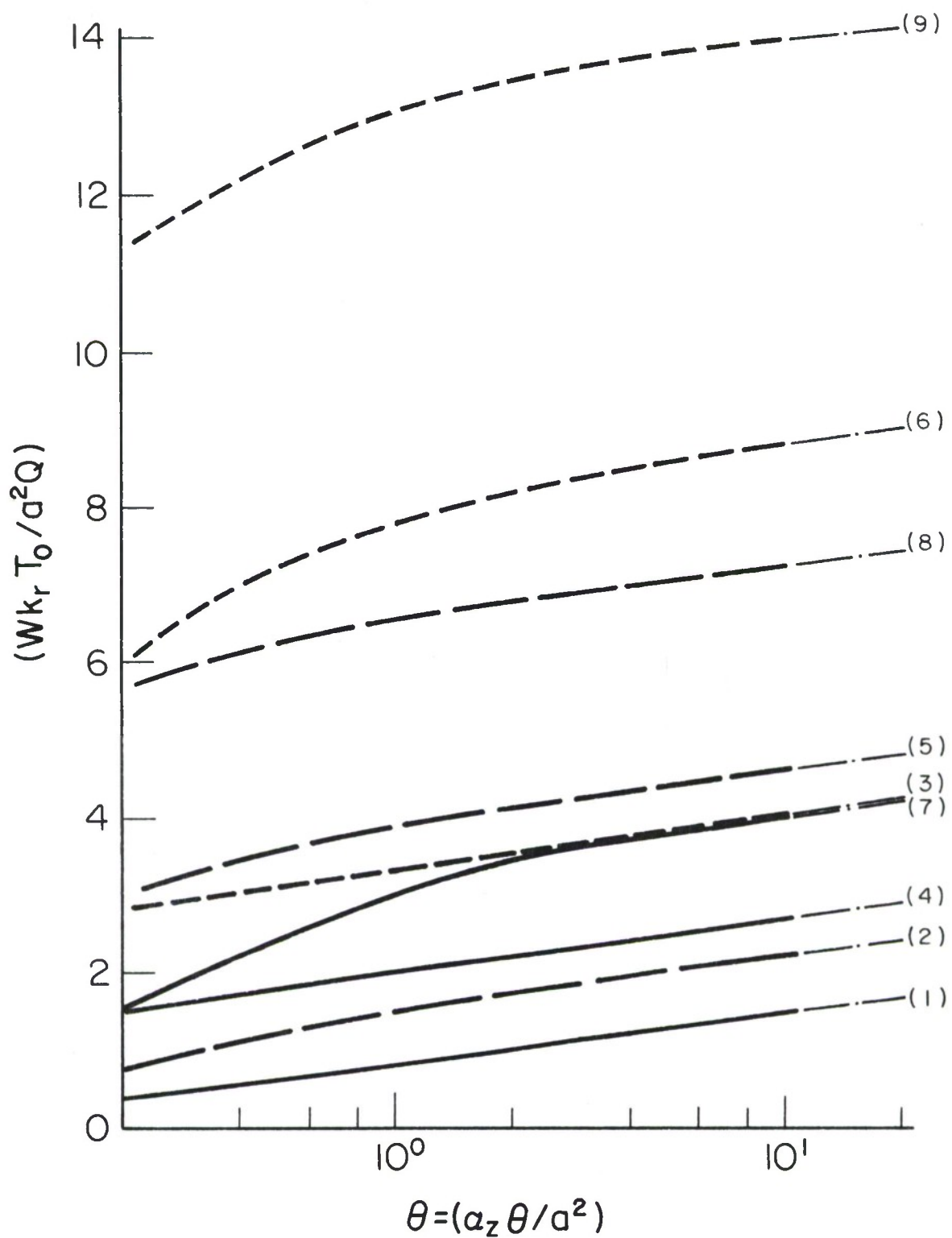


Figure 9. Asymptotic Variations of Heat Spot Temperature Rises

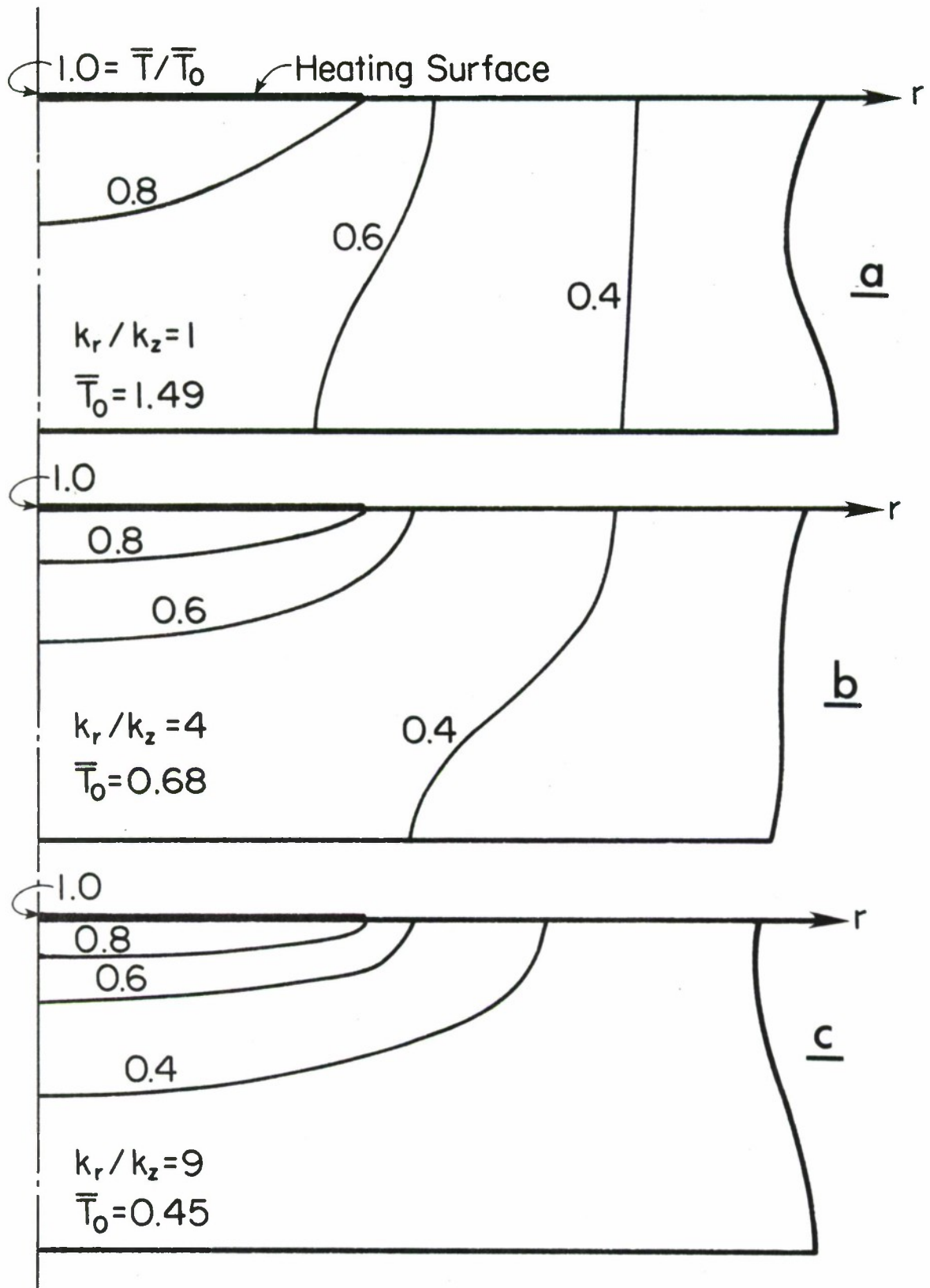


Figure 10. Spot Heating Isothermal Contours at Various Conductivity Ratios, $w/a = 1$

Shown in Figure 10 are isothermal contours which define temperature rises corresponding to 0.8, 0.6, and 0.4 of the individual hot spot temperature rises for the cases of $k_r/k_z = 1, 4, \text{ and } 9$; all for $w/a = 1$. For the case of $k_r/k_z = 1$ shown in Part (a) of Figure 10, the temperature contours beyond the heating beam radius of a are nearly transverse to the slab; this is of course indicative of near one-dimensional temperature distributions in which the distribution is asymptotic, gradually approaching that of Figure 7. For larger in-plane thermal conductivities, $k_r/k_z = 4$ and 9 , temperature contours shown in Parts (b) and (c) of Figure 10 signify higher radial (in-plane) spread than in the depth direction. Not only is the back surface temperature reduced by rapid heat dissipation near the heat-input surface, but more so is the temperature rise of the surface heat spot itself. At heating time $\bar{\theta} = 10$, for which Figure 10 is valid, the spot-center temperatures for the three conductivity ratios are 1.49, 0.68 and 0.45, respectively. This observation is most significant when the criterion of burn-through of thermal shields is considered.

Similar to the contours in Figure 10, the cases of $w/a = 4$ and $k_r/k_z = 1$ and 9 are displayed in Figures 11 and 12. For isotropic conductivity, the contours (Figure 11) at $\bar{\theta} = 10$ are very nearly circular (spherical in reality), as would be expected; in contrast, for $k_r/k_z = 9$, temperature rises are concentrated near the heat source but spread appreciably along the plane, resulting in contours of flat ellipses.

Another feature of significance is the profile of the slab temperature on the heat input surface $\bar{z} = 0$; Figures 13 and 14 show the lateral

temperature variations for $k_r/k_z = 1$ and 9, each with $w/a = 1$ and 4, respectively, in these two illustrations. As in the case of the isothermal contours, the temperature profiles are presented in terms of their ratios to the temperature of the heat spot center. In spite of wide variations of the parameters (w/a) from 1 to 4 and the conductivity ratio (k_r/k_z) from 1 to 9, the surface temperature profiles are remarkably similar to each other: a very nearly flat region within the beam radius and sharp drop from the beam edge outward. It is particularly worth noting that the temperature at the beam edge is approximately 0.8 of the temperature at beam center and the temperature ratio is reduced to 0.3 at a distance of two radii from the center. The former relation is used in correlating the surface temperature rise with the asymptotic heat flow configuration of Figure 7 and equation (34).

2.5 Summary and Recommendations

At the end of $\bar{\theta} = 10$, the heat beam center temperatures and the back temperatures for the nine combinations of parameters are listed in Table I. Starting with the case of $k_r/k_z = 1$ and $w/a = 1$, the heat beam spot temperature is reduced from 1.49 to 1.015 by increasing the thickness to $w/a = 4$. However, a greater reduction of the surface temperature can be achieved by increasing the in-plane thermal conductivity: By using $k_r/k_z = 4$ and 9, the surface temperature becomes 0.682 and 0.450 respectively. This observation demonstrates the need for composites with larger in-plane thermal conductivities than the transverse values.

Aside from concluding that the in-plane thermal conductivities of composite labs have a predominant influence on the thermal responses in general, this investigation also demonstrates other typical analyses among many needed for a survivability and vulnerability evaluation of protective materials. The types of investigations needed can be, broadly speaking, classified into (i) short-term damages characterized by imminent incapacitation, such as burn-through melting, large-deformation buckling and fracture and (ii) long-term cumulative damages, such as thermally-induced stress concentration around voids, cracks, and delamination of layers, etc. Indeed, the analysis of spot-heating treating in this report -- even though limited to the temperature effect along -- belongs to the first category, for if the heating process continues, burn-through or pit-forming is the next stage of occurrence.

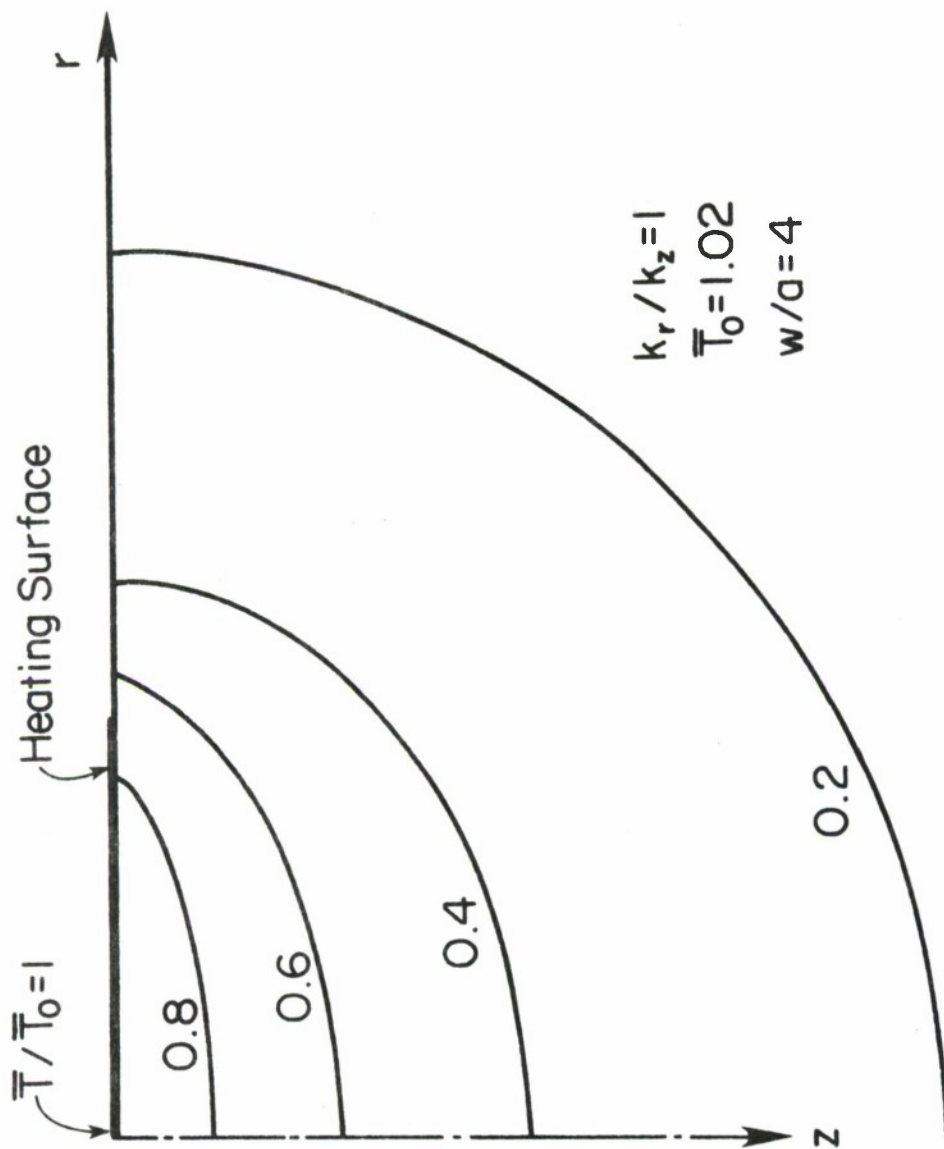


Figure 11. Spot Heating Isothermal Contours for $w/a = 4$ and $k_r/k_z = 1$

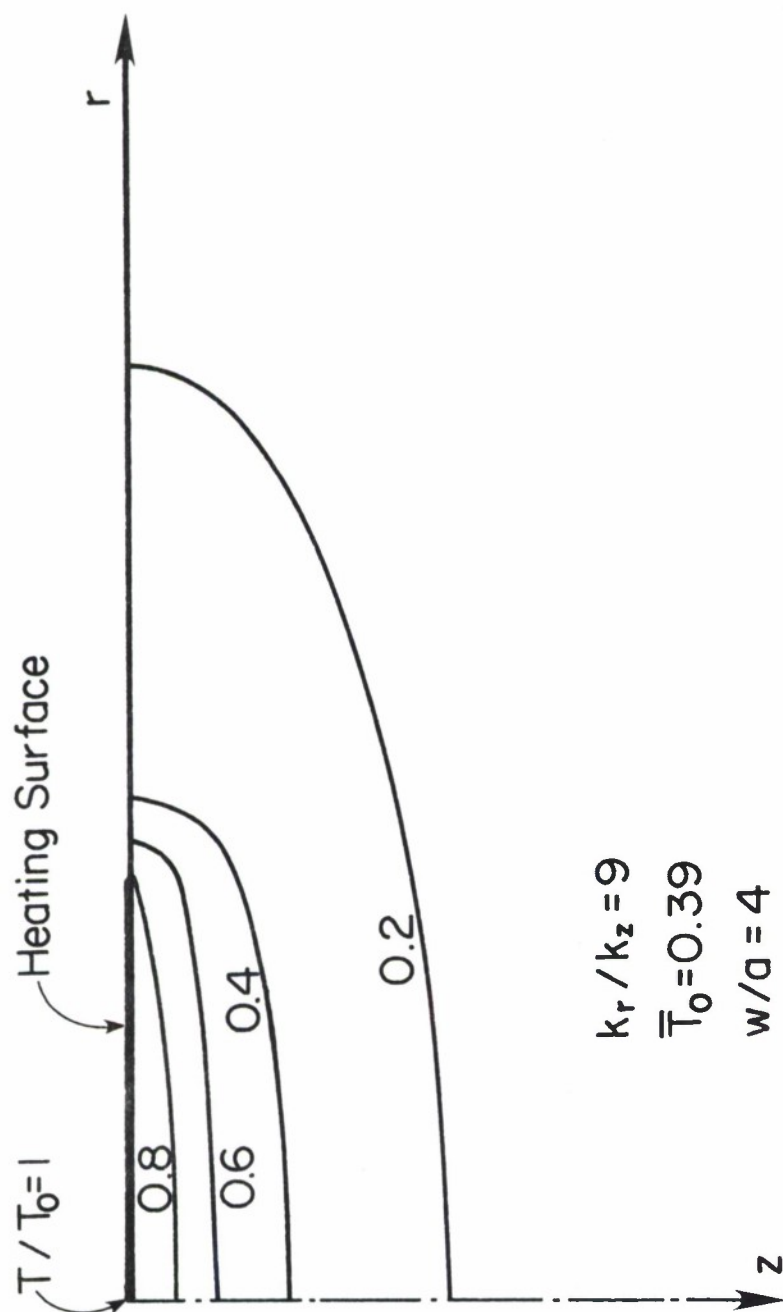


Figure 12. Spot Heating Isothermal Contours for $w/a = 4$ and $k_r/k_z = 9$

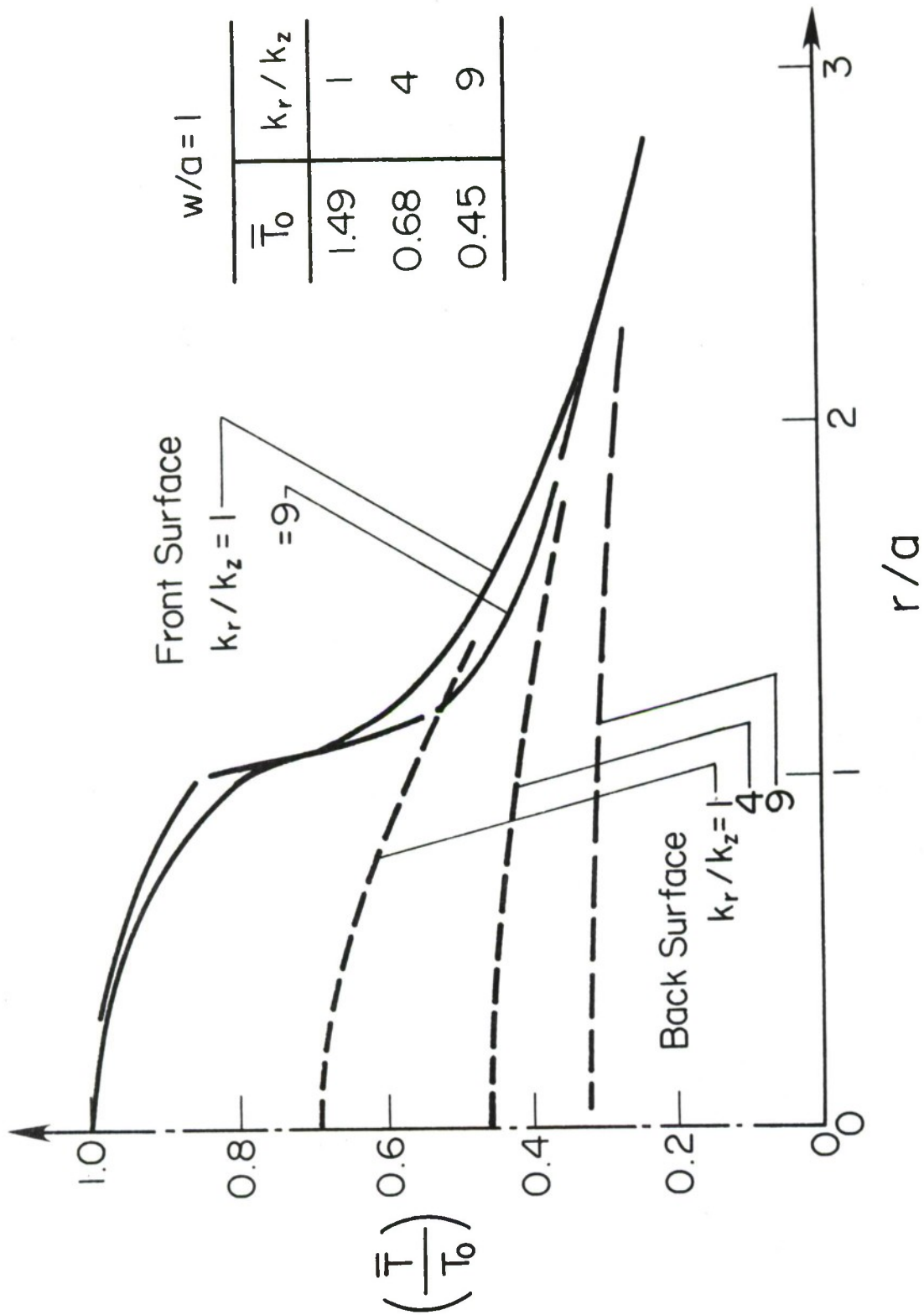


Figure 13. Surface Temperature Profiles at Various Conductivity Ratios, $w/a = 1$

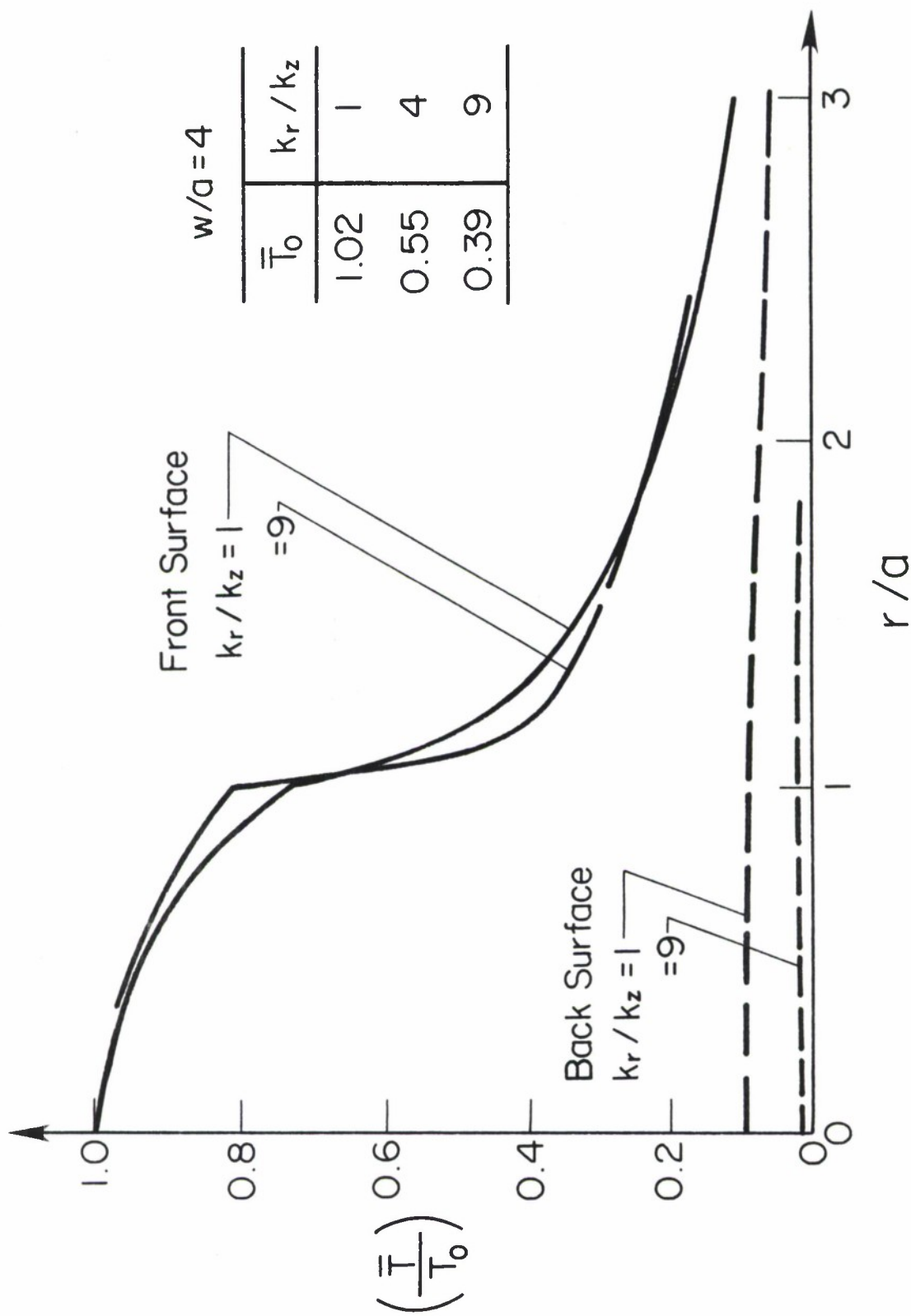


Figure 14. Surface Temperature Profiles at Various Conductivity Ratios, $w/a = 4$

Table I. Calculated Heat Spot and Back Temperatures*

($\bar{\theta} = 10$)

(k_r/k_z)	$w/a = 1$	$w/a = 2$	$w/a = 4$
1	1.495	1.121	1.015
	1.026	0.395	0.107
4	0.682	0.578	0.550
	0.305	0.106	0.028
9	0.450	0.402	0.388
	0.142	0.048	0.009

* The top and bottom figures indicate the frontal and back surface temperatures respectively; the temperature is defined by

$$\bar{T} = k_z T/aQ.$$

3. TRANSIENT HEAT FLOW IN MULTI-LAYERED COMPOSITES

Aside from the axis-symmetrical spot-heating problem analyzed and discussed in the preceding section, one-dimensional transient heating of multi-layered composites constitutes a fundamental class of problems -- not necessarily from the viewpoint of its novelty or difficulty -- but from the viewpoint of providing realistic temperature distributions throughout the composite bulk so that the resultant thermal stresses can be calculated based on more realistic thermal analyses.

The first problem of transient conduction analyzed in this part of the report is the heating by a constant heat flux of a multi-layered composite panel. From a vulnerability standpoint, assessment of composites used in space structure must, by necessity, involve the constant heat flux criterion in order to establish the temperature excursion which a candidate composite structure may undergo. In this connection, relevant parameters are the heat flux intensity, its duration, and the thermal properties of the composite materials. The temperature responses derived therefrom constitute the input to the next phase of analysis for the resulting thermal stresses and possible deformation, buckling, etc., which are based on known material thermoelastic properties and the geometrical specification of the space structural shape.

The second problem discussed in this section pertains to the periodic heating and cooling which comes about, for example, in an orbiting space structure. During a portion of its cycle, solar irradiation raises the exposed surface temperature and during its stay in the shadow, the surface temperature lowers. The cyclic surface

temperature fluctuation is a direct consequence of the fluctuating surface heat flux about its cyclic average value. Such a periodic heat flux variation and surface temperature excursion are of course mutually convertible and can be expressed by a Fourier series whose basic period is the orbiting time, with higher harmonics taking into account irregularities from a sine-wave representation.

The development herein focuses more on the methodology which is heretofore unavailable than on the complex parameters involved in an orbiting event. From an application viewpoint, the method of analysis easily accessible in this report makes the cyclic temperature analysis possible for composites with any number of layers. Given the relevant parameters of the heat flux intensity, etc., the computed temperature fluctuations throughout the body of the composite naturally lead to more realistic determinations of internal thermal stresses and strains.

3.1 Impulsive Surface Heat Flux

Even though the development is applicable to composite panels composed of any number of layers, the mathematical development and numerical presentation are limited to a two-layer configuration for simplicity and compactness. Figure 15 depicts an inner layer, substrate *s* or layer number 1, protected by an outer layer, coating *c* or layer number 2, which acts as a thermal shield. With *c* and *s* as subscripts, the governing diffusion equations in these two regions are

$$k_c \frac{\partial^2 T_c}{\partial x^2} = (\rho C)_c \frac{\partial T_c}{\partial \theta} \quad (35)$$

$$k_s \frac{\partial^2 T_s}{\partial x^2} = (\rho C)_s \frac{\partial T_s}{\partial \theta} \quad (36)$$

At the exposed surface, a constant heat flux Q is imposed impulsively on the composite panel, which has an initial temperature of zero everywhere. On the back surface of the substrate region, an insulated boundary condition is assumed. Between the two regions, the conditions of equal temperatures and equal heat fluxes are naturally valid. Altogether, these boundary conditions are

$$\frac{\partial T_s}{\partial x} = 0 \quad (x = 0) \quad (37)$$

$$k_c \frac{\partial T_c}{\partial x} = Q \quad (x = L_t) \quad (38)$$

$$T_s = T_c \quad (x = L_s) \quad (39)$$

$$k_s \frac{\partial T_s}{\partial x} = k_c \frac{\partial T_c}{\partial x} \quad (x = L_s) \quad (40)$$

By using non-dimensional variables defined by,

$$\left. \begin{aligned}
 \bar{x} &= x/L_t \\
 \bar{\theta} &= \alpha_s \theta / L_t^2 \\
 \bar{T}_s &= k_s T_s / (Q L_t) \\
 \bar{T}_c &= k_s T_c / (Q L_t) \\
 \bar{L}_s &= L_s / L_t
 \end{aligned} \right\} \quad (41)$$

the governing equations and their associated boundary conditions become:

$$\frac{\partial^2 \bar{T}_s}{\partial \bar{x}^2} = \frac{\partial \bar{T}_s}{\partial \bar{\theta}} \quad (42)$$

$$\frac{\alpha_c}{\alpha_s} \frac{\partial^2 \bar{T}_c}{\partial \bar{x}^2} = \frac{\partial \bar{T}_c}{\partial \bar{\theta}} \quad (43)$$

$$\frac{\partial \bar{T}_s}{\partial \bar{x}} = 0 \quad (\bar{x} = 0) \quad (44)$$

$$\frac{k_c}{k_s} \frac{\partial \bar{T}_c}{\partial \bar{x}} = 1 \quad (\bar{x} = 1) \quad (45)$$

$$\bar{T}_s = \bar{T}_c \quad (\bar{x} = \bar{L}_s) \quad (46)$$

$$\frac{\partial \bar{T}_s}{\partial \bar{x}} = \frac{k_c}{k_s} \frac{\partial \bar{T}_c}{\partial \bar{x}} \quad (\bar{x} = \bar{L}_s) \quad (47)$$

The group of equations (42) through (47) indicates that the transient solutions of T_s and T_c are dependent upon two parameters: the ratio of the diffusivities (α_c/α_s) and the ratio of the conductivities (k_c/k_s).

Finite-Difference Formulation. Numerical solution of equations (42) through (47) is most conveniently accomplished by a one time-step forward marching process in conjunction with 3-point space derivatives. Although the problem can be solved analytically, the resulting formulation in terms of segmental eigenfunctions becomes too unwieldy to handle. Numerical treatment appears to be the most expedient approach. As in the case of the spot-heating problem, the ADE-method (time-splitting) is used to insure speed and accuracy. Based on a uniform grid size of $\Delta\bar{x}$, the time step for satisfying numerical stability is governed by the following:

$$\Delta\bar{\theta} < (\Delta\bar{x})^2 (\alpha_s/\alpha_c) \quad (48)$$

$$\Delta\bar{\theta} < (\Delta\bar{x})^2 \quad (49)$$

which are equivalent to the Neuman's stability formulation for each region.

In the computations carried out in this analysis, the minimum time deduced from these two criteria is further reduced by one half to insure accuracy. The space grid size $\Delta\bar{x}$ is determined by requiring the thinner layer of the two to have a minimum of 10 divisions. The use of the subscripts c and s is dropped, for the different regions can be distinguished by referring to the index of the temperature node in the arrayed notations. By using the ADE-method, which is in essence a split-time technique, equations (42) and (43) are replaced by a single finite-difference formula:

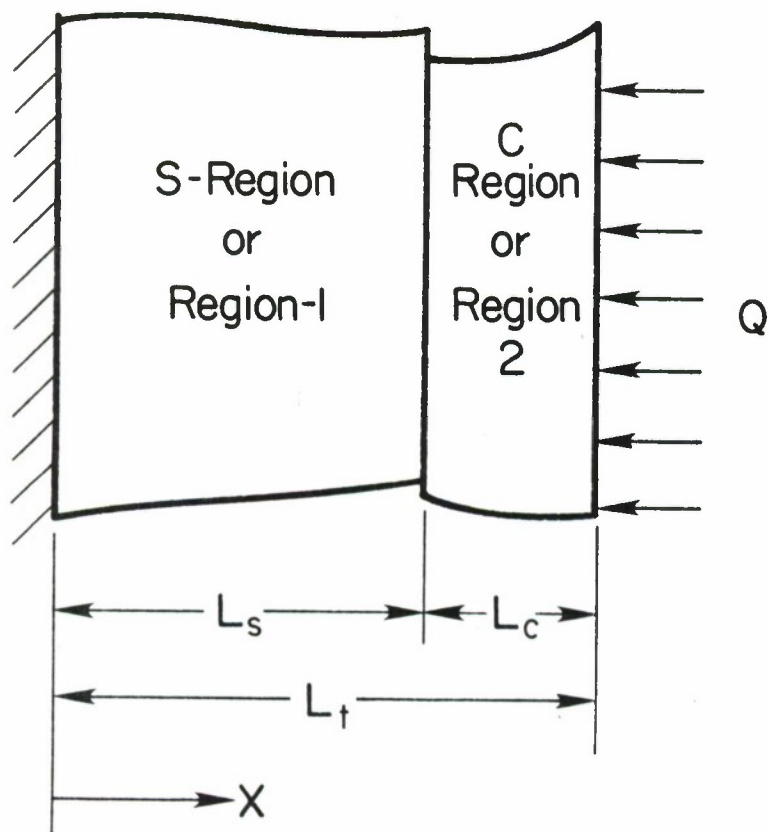


Figure 15. Two-Layer Composite Configuration and Definitions

$$T_i^n = \frac{\lambda [T_{i+1} + T_{i-1}] + (1 - \lambda) T_i}{(1 + \lambda)} \quad (50)$$

where:

i = index number of the node ($i = 1$, heating surface)

$\lambda = (\alpha_c / \alpha_s) \Delta \bar{\theta} / (\Delta \bar{x})^2$, in c-region

$\lambda = \Delta \bar{\theta} / (\Delta \bar{x})^2$, in s-region

and subscript n denotes the value at a later time-step. The node index i starts from the heating surface $\bar{x} = 1$, $i = 1$ and increases towards the insulation surface of $\bar{x} = 0$.

The heating boundary condition at $\bar{x} = 1$ ($i=1$) is expressed, through a three-point differentiation approximation, by

$$T_1^n = [4T_2 - T_3 + 2(\Delta \bar{z})(k_s/k_c)]/3 \quad (51)$$

The interfacial boundary condition is similarly obtained as

$$T_6^n = \frac{[(4T_7 - T_8)(k_s/k_c) + (4T_5^n - T_4^n)]}{[3 + 3(k_s/k_c)]} \quad (52)$$

where the node numbers are sequential from right to left with node number 6 at the interface. The use of these numerals is of course illustrative only. Again the superscripted quantities denote values at

a later time-step, but they become known in the forward sweep algorithm. Using the same strategy, the end temperature at $\bar{x} = 0$ is calculated by:

$$T_6^n = [4T_5^n - T_4^n]/3 \quad (53)$$

where node number 6 is used simply to illustrate the end point.

Results and Discussion. The calculated results are expressed in terms of T_c and T_s at the nodal points as time proceeds. Of these, the most significant are at the front, interface and back positions, i.e., $\bar{x} = 1$, $\bar{x} = \bar{L}_s$, and $\bar{x} = 0$. From a phenomenological viewpoint, all temperatures increase with time and eventually become linearly dependent upon it. However, for the purpose of analyzing various coatings in protecting the substrate layer, the relative magnitudes of the substrate temperatures at a fixed heating rate Q for a fixed duration θ become an important criterion in coating selection.

In the numerical computations undertaken, values of the coating thermal conductivity relative to that of the substrate layer are assumed as 0.2, 0.5 and 1. These are low-conductivity coatings used as thermal insulators. For the first set of calculations, the product (ρC) of the coating is made equal to that of the substrate layer. The relative effectiveness of the coatings can therefore be judged by examining the temperature rises of the substrate temperatures at $\bar{x} = \bar{L}_s$ and at $\bar{x} = 0$. The coating thickness is taken to be 0.25 of the substrate thickness. Results of this set of calculations are shown in Figure 16, where the temperature rises of the substrate surface temperatures at $\bar{x} = \bar{L}_s$ are grouped together for coatings of conductivity ratios of 0.2 and 0.5 and

1. The closeness of the distribution curves suggests that coatings with low thermal conductivities are only mildly effective in protecting the substrate surface. The reason is, of course, that in the case of a constant heat flux the coating surface temperature rises more steeply when its conductivity is low and vice versa; the end result is that at the interface with the substrate, the temperature changes with time are not materially different for conductivity ratios of 0.2 to 1. The preceding observation is not valid if the heating environment is that of convection.

Another set of calculations was carried out with the coating conductivity equal to that of the substrate but with their thermal capacity (ρC) ratios of 1, 1.5, 2, and 4. Results of varying the thermal capacity ratio indicate that the surface temperature of the substrate is substantially reduced by using coatings with high (ρC) values and the effect is much more pronounced than it is when using coatings of lower thermal conductivities.

Figure 17 displays the front surface temperatures of the substrate with coatings of various thermal capacity ratios. The back surface temperature variations with time are shown in Figure 18. Notable differences among these response curves are maintained along the time scale, contrary to those in Figure 16. Hence coatings with high relative (to substrate) values of (ρC) are much more effective than coatings of low k -values. Of course, combinations of the two factors enhance the effectiveness of protection. Thus in relation to the substrate properties, coatings with thermal diffusivities lower than the substrates' are preferred thermal shields.

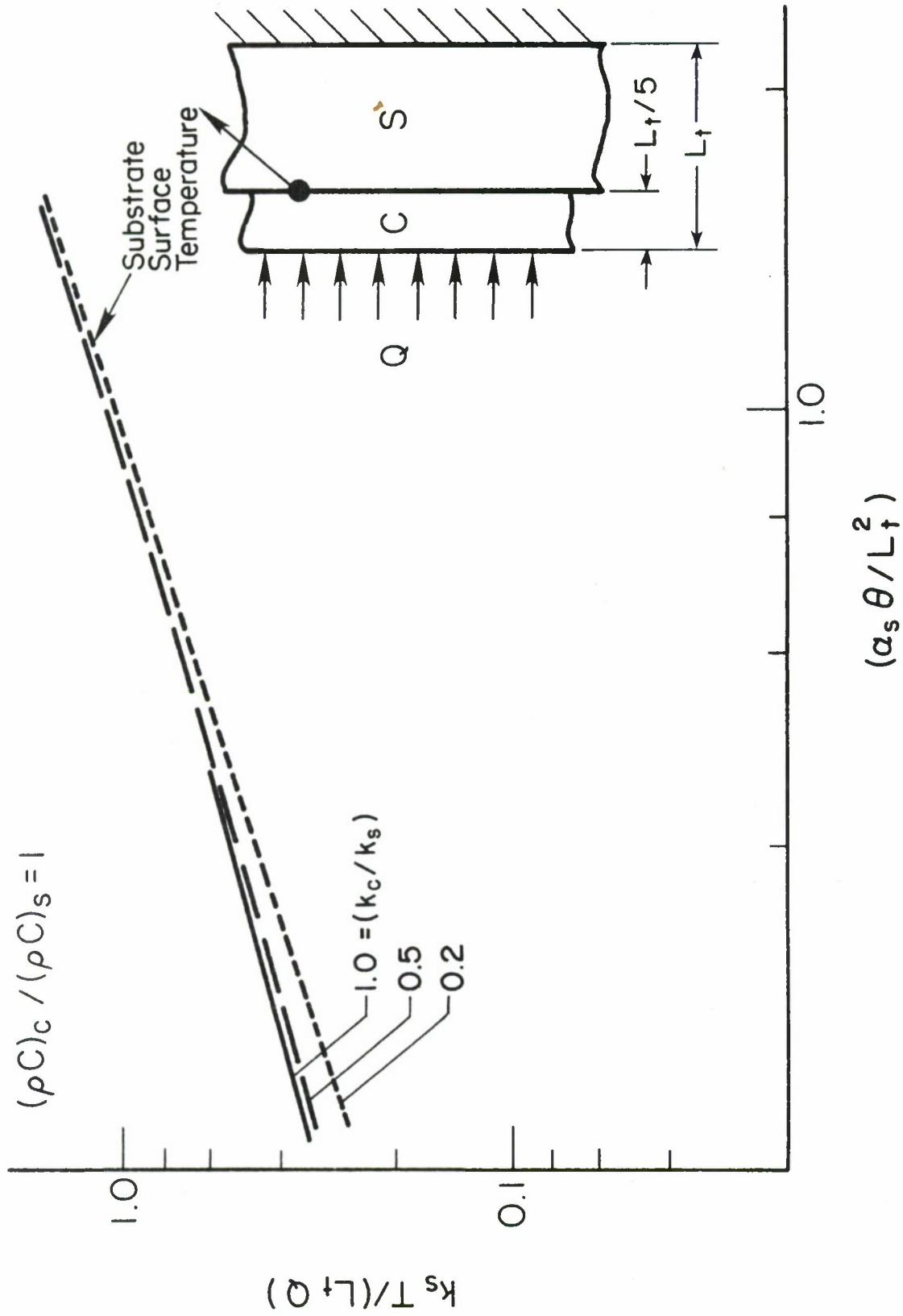


Figure 16. Interface Temperature Rises Due to Constant Heat Flux at Various Coating Conductivities

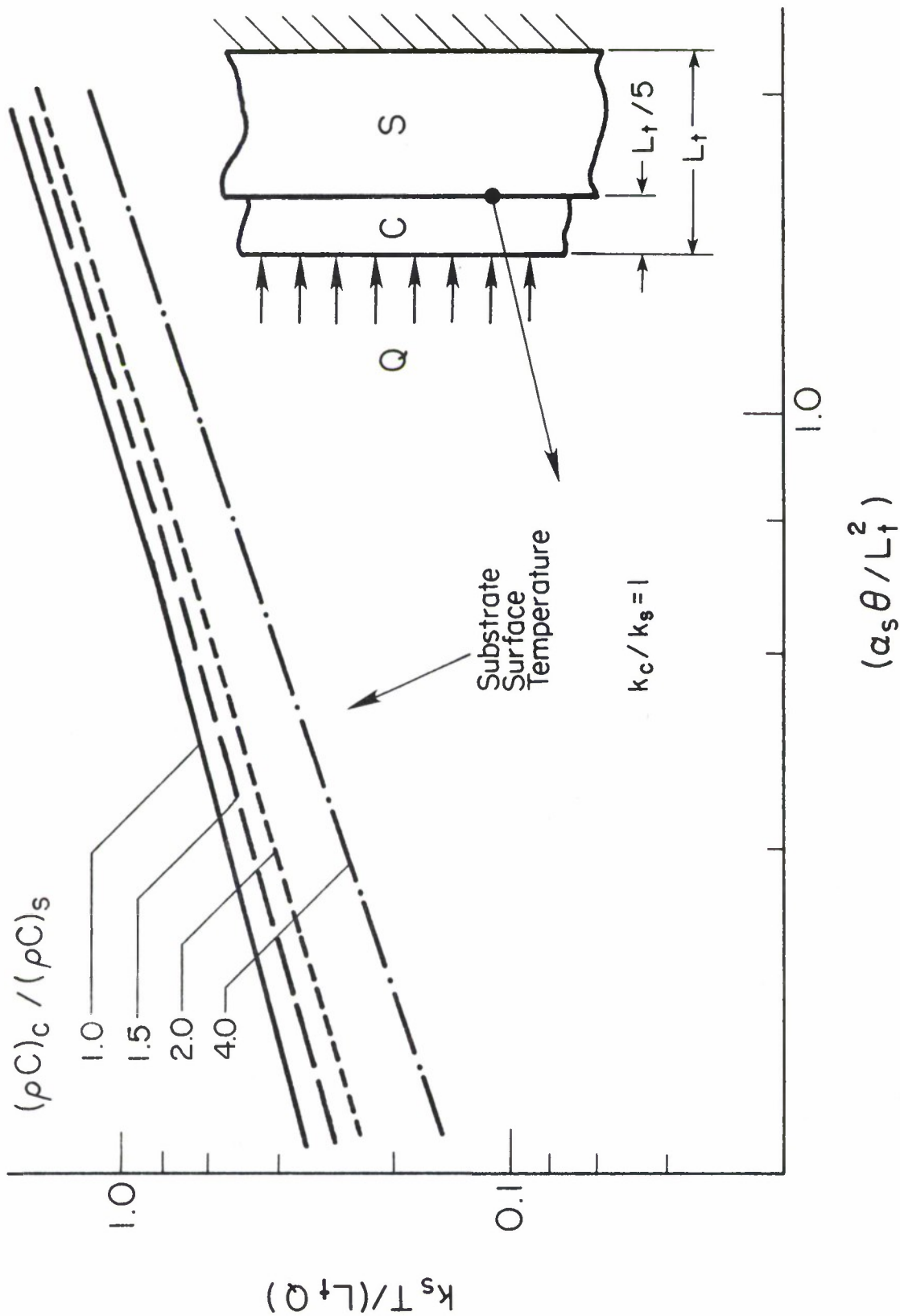


Figure 17. Interface Temperature Rises Due to Constant Heat Flux at Various Coating Thermal Capacity Ratios

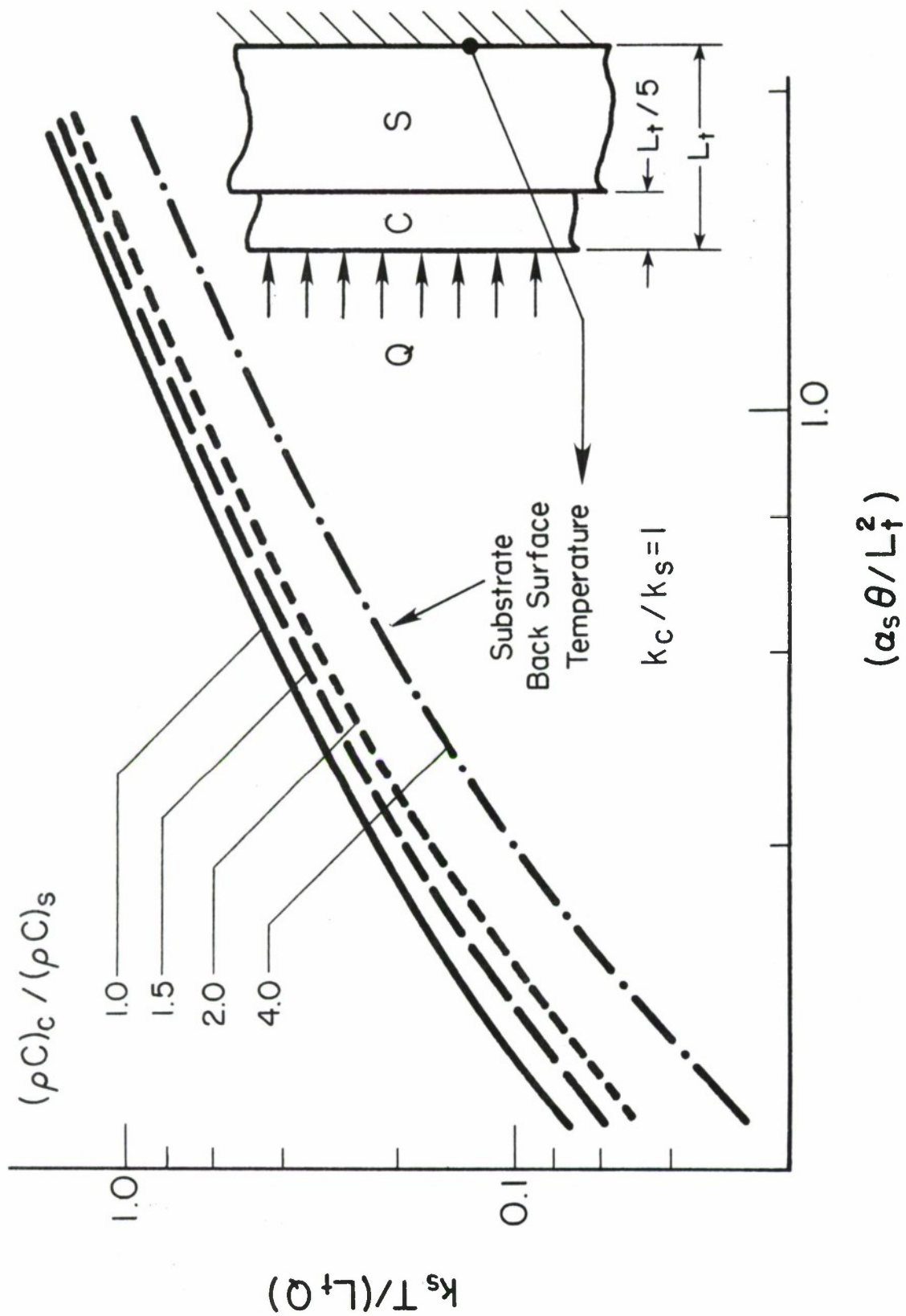


Figure 18. Back Surface Temperature Rises Due to Constant Heat Flux at Various Coating Thermal Capacity Ratios

3.2 Cyclic Surface Temperature

A space structural component, when subjected to a cyclic surface temperature, may exhibit little internal temperature variation while the internal temperature level follows almost in parallel with the imposed surface temperature fluctuation. This occurs when the surface temperature cycle is long and the internal heat flow resistance is low. It follows naturally that when the surface variation is rapid in its fluctuation coupled with large internal thermal resistance, there would be considerable internal temperature variation throughout its bulk with larger temperature excursions near the heating surface. In the above description, heating by cyclic surface temperature variation or by cyclic surface heat flux is considered identical, for one situation can be readily converted into the other by the spatial gradient of the former case.

The governing criterion for these two extremes is the two relative time scales: the physical cyclic time and the thermal diffusion time; the former stems from the imposed boundary condition and the latter is an intrinsic property of the material medium. Compounding the situation is, of course, the multi-layer nature of a composite, which makes the analysis complicated. From a technical viewpoint, the problem may be stated as follows: given a surface temperature cycle history, determine the steady-state cyclic temperature variation of a multi-layered composite for which thermal properties are known a priori. Answers to this

question are of significance in determining the cyclic thermal growth of composites and sequentially the thermal fatigue stress a component may experience.

It turns out that numerical analysis by the finite-difference or finite-element method is not the approach to use, for the focus is on the steady-state cyclic temperature responses. By numerical methods, solutions would not be forthcoming until the temperature cycle becomes periodic and repeating. In principle it is possible; in practice it is not feasible to implement for all kinds of combinations of problem specifications. Thus analytical tools are resorted to.

Analysis. Consider a multi-layered composite depicted in Figure 19. Starting from $\bar{x} = 0$, the layers are numbered 1 to n, each having thermal properties distinct from other layers. At the last layer (layer n), the exposed surface has a boundary condition described by a cyclic temperature fluctuation about a mean value. The cyclic part may be expressed by

$$T_s = \sum_{m=1}^{\infty} \left[A_m \cos \omega_m \theta + B_m \sin \omega_m \theta \right] \quad (54)$$

Since constant (independent of temperature) thermal physical properties are assumed, the entire problem is a linear one. Hence in equation (54), only a representative term needs to be considered; accordingly, a typical term is detached from equation (54) and is taken as the boundary condition at $\bar{x} = \bar{L}_n$. The conditions of equal temperatures and heat fluxes naturally apply at the interfacial positions.

Denoting the temperature responses (from a mean value) as $T_1, T_2, \dots T_n$ for these layers, the individual diffusion equations can be expressed by an indexed notation as

$$\frac{\partial^2 T_j}{\partial x^2} = \frac{1}{\alpha_j} \frac{\partial T_j}{\partial \theta} \quad (55)$$

for $j = 1, \dots n$. Using the total thickness L_n as the reference length and the physical properties of the first layer (1) as reference, the following non-dimensional variables are defined:

$$\bar{x} = (x/L_n) \quad (56)$$

$$\bar{\theta} = (\alpha_1 \theta / L_n^2)$$

The governing equations for each layer become

$$\frac{\partial^2 T_j}{\partial \bar{x}^2} = \frac{\alpha_1}{\alpha_j} \frac{\partial T_j}{\partial \bar{\theta}} \quad (57)$$

The interfacial positions are defined by

$$\bar{x} = \bar{L}_1, \bar{L}_2 \dots \bar{L}_{n-1}$$

with $\bar{L}_n = 1$ for the exposed surface, at which the temperature of the last layer is specified by

$$T_{n(\bar{x}=1)} = A \cos \bar{\omega}\bar{\theta} + B \sin \bar{\omega}\bar{\theta} \quad (58)$$

or

$$T_{n(\bar{x}=1)} = (A/2)(e^{i\bar{\omega}\bar{\theta}} + e^{-i\bar{\omega}\bar{\theta}}) - (iB/2)(e^{i\bar{\omega}\bar{\theta}} - e^{-i\bar{\omega}\bar{\theta}}) \quad (59)$$

(Note that the surface temperature variation in equation (58) has been expressed in terms of the non-dimensional diffusion time θ with a corresponding change of ω to $\bar{\omega}$ which will be discussed later.) To determine the periodic solution for the j -th layer between $\bar{x} = \bar{L}_{j-1}$ to $\bar{x} = \bar{L}_j$, a reference solution is obtained which satisfies the surface temperature fluctuation $(A/2)e^{i\bar{\omega}\bar{\theta}}$. Let this solution be called A-solution; then the complete solution of the j -th layer due to $A \cos \bar{\omega}\bar{\theta}$ is the A-solution plus its complex conjugate. To obtain the solution due to $B \sin \bar{\omega}\bar{\theta}$, the reference A-solution is changed, (by replacing A by $-iB$) into B-solution. The complete solution due to the surface temperature $B \sin \bar{\omega}\bar{\theta}$ is therefore B-solution minus its complex conjugate.

A-Solution. To obtain the solution T_j , for the j -th layer, consider the substitution

$$T_{A-j} = (A/2)e^{i\bar{\omega}\bar{\theta}} e^{\beta_j \bar{x}} \quad (60)$$

which upon substitution into equation (57) gives the exponential constant β_j as

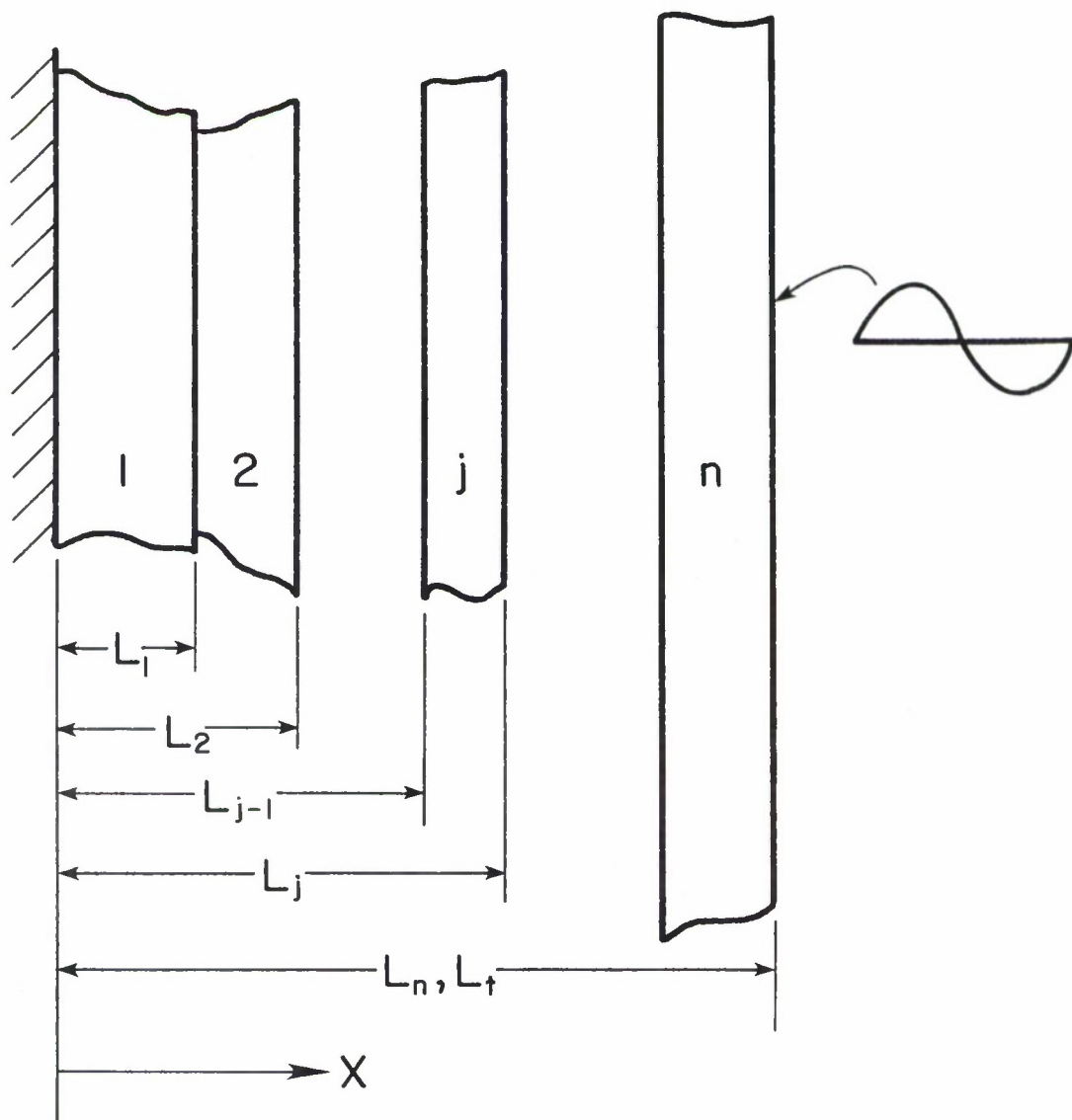


Figure 19. Multi-Layer Panel Configuration and Definitions

$$\beta_j = \sqrt{(\alpha_1/\alpha_j)(\omega/2)}(1+i) \quad (61)$$

For the first layer whose inner surface at $\bar{x} = 0$ is insulated against heat conduction, equation (60) can be written as

$$T_{A-1} = (A/2)e^{i\bar{\omega}\bar{\theta}} \left[G_1 \cosh \beta_1 \bar{x} \right] \quad (62)$$

where G_1 is a complex constant. Note that equation (62) already satisfies the zero-gradient requirement at $\bar{x} = 0$. For layers from no. 2 on, the solutions can be expressed by

$$T_{A-j} = (A/2)e^{i\bar{\omega}\bar{\theta}} \left[G_j \cosh \beta_j (\bar{x} - \bar{L}_{j-1}) + H_j \sinh \beta_j (\bar{x} - \bar{L}_{j-1}) \right] \quad (63)$$

$j \geq 2$

The functional form in equation (63) differs from the more elementary form of equation (60) for the reason that equation (57) permits simple deduction of the coefficients G_j and H_j . Noting that equation (63) applies for \bar{x} between \bar{L}_{j-1} and \bar{L}_j , the starting value of the terms inside the brackets is simply G_j which therefore equals the end value of the preceding layer no. (j-1). In addition, since the first term of equation (63) has its gradient zero at the starting position $\bar{x} = \bar{L}_{j-1}$, the second term has a gradient of $H_j \beta_j$ which must therefore be related to the gradient of the preceding solution at its end-point. In this way the calculation procedure can be made sequential and simple in its algorithm. By proceeding from the inner most layer 1 to the outermost layer n, the coefficients G_j and H_j can be easily determined in terms

of their ratios to the first coefficients G_1 . At the surface position $\bar{x} = 1$, where the surface temperature $(A/2)e^{i\omega\theta}$ must be satisfied, the equation determining the first constant G_1 then becomes

$$G_1 \left[\left(\frac{G_n}{G_1} \right) \cosh \beta_n (1 - \bar{L}_{n-1}) + \left(\frac{H_n}{G_1} \right) \sinh \beta_n (1 - \bar{L}_{n-1}) \right] = 1 \quad (64)$$

where the ratios (G_n/G_1) and (H_n/G_1) are known, having been determined by proceeding from layer to layer.

The A-solution for the $(A/2)e^{i\omega\theta}$ -surface temperature perturbation is therefore embedded in equation (63), which contains complex coefficients G_j and H_j for the j -th layer of the composite. Expressing the solution in the form of

$$T_{A-j} = (A/2)e^{i\omega\bar{\theta}} [R_j + iI_j] \quad (65)$$

where R_j and I_j are respectively the real and imaginary parts of the complex function in equation (63), equation (65) can be expressed in a more elementary form:

$$T_{A-j} = \frac{A}{2} [(R_j \cos \bar{\omega}\bar{\theta} - I_j \sin \bar{\omega}\bar{\theta}) + i (R_j \sin \bar{\omega}\bar{\theta} + I_j \cos \bar{\omega}\bar{\theta})] \quad (66)$$

The complete solution due to a surface temperature fluctuation of $A \cos \omega\theta$ is therefore the sum of T_{A-j} plus its complex conjugate, and is consequently

$$T_A = A [R_j \cos \bar{\omega}\bar{\theta} - I_j \sin \bar{\omega}\bar{\theta}] \quad (67)$$

where j is the layer number. Again, R_j and I_j are the real and imaginary parts of the G- and H-terms in equation (63).

B-Solution. To the surface temperature variation $B \sin \omega \theta$, there is a corresponding temperature response for each layer. By virtue of equation (59), the temperature response to $(-iB/2)e^{i\omega\theta}$ is simply the response to $(A/2)e^{i\omega\theta}$ if A is replaced by $(-iB)$. This is the B-Solution. Using equation (66) as the model, the B-Solution can be expressed by

$$T_{B-j} = \frac{-iB}{2} \left[(R_j \cos \bar{\omega}\bar{\theta} - I_j \sin \bar{\omega}\bar{\theta}) + i(R_j \sin \bar{\omega}\bar{\theta} + I_j \cos \bar{\omega}\bar{\theta}) \right] \quad (68)$$

Finding its complex conjugate and subtracting it from T_{B-j} gives the temperature response function T_B for the j -th layer as

$$T_B = B[R_j \sin \bar{\omega}\bar{\theta} + I_j \cos \bar{\omega}\bar{\theta}] \quad (69)$$

Solution for Two-Layer Composites. For a composite panel consisting of two layers, the solution is not unduly complicated and can be obtained by using equation (62) and equation (63) with $j = n = 2$. At the interfacial position, $\bar{x} = \bar{L}_1$, $T_{A-1} = T_{A-2}$. Therefore,

$$(G_2/G_1) = \cosh \beta_1 \bar{L}_1 \quad (70)$$

The equal heat flux condition at $\bar{x} = \bar{L}_1$, becomes

$$(H_2/G_1) = \frac{k_1 \beta_1}{k_2 \beta_2} \sinh \beta_2 \bar{L}_1 \quad (71)$$

Introducing G_2/G_1 and H_2/G_1 into equation (63) for $j = 2$ and setting $\bar{x} = 1$, an expression for the fluctuating outer surface temperature is obtained. The required boundary condition is met by setting

$$G_1 [(G_2/G_1) \cosh \beta_2 (1 - \bar{L}_1) + (H_2/G_1) \sinh \beta_2 (1 - \bar{L}_1)] = 1 \quad (72)$$

The first complex coefficient β_1 along with G_2 and H_2 , is therefore determined. With the coefficients known, the temperature fluctuation can be separated into R and I parts in the region occupied by each layer. The complete expressions for layers 1 and 2 are therefore:

$$T_{A-1} = (A/2) e^{i\bar{\omega}\bar{\theta}} [\cosh \beta_1 \bar{x}] G_1 \quad (73)$$

$$T_{A-2} = (A/2) e^{i\bar{\omega}\bar{\theta}} \left[\cosh \beta_1 \bar{L}_1 \cosh \beta_2 (\bar{x} - \bar{L}_1) + \sqrt{\frac{k_1 \rho_1 c_1}{k_2 \rho_2 c_2}} \sinh \beta_1 \bar{L}_1 \sinh \beta_2 (\bar{x} - \bar{L}_1) \right] G_1 \quad (74)$$

where G_1 is given by equation (72).

Diffusivity-Cycle Frequency $\bar{\omega}$ and Computational Results.

In the specification of surface temperature variation with time, a circular frequency ω is used in conjunction with θ , as in equation (54). In non-dimensional coordinates, however, diffusivity-referenced time

is used, as defined by equation (56), which necessitates the use of a non-dimensional frequency $\bar{\omega}$. Its definition can be established by considering the identity $\omega\theta = \bar{\omega}\bar{\theta}$; hence

$$\bar{\omega} = \omega L_t^2 / \alpha_1$$

Since in the physical coordinates, the circular frequency ω is related to the fundamental period P by $\omega = 2\pi/P$, the non-dimensional diffusion-cycle frequency $\bar{\omega}$ is given by

$$\bar{\omega} = 2\pi L_t^2 / \alpha_1 P \quad (75)$$

which becomes a key parameter in the analysis of periodic temperature responses of composites.

Its approximate magnitude in a typical structural application can be established by considering a low earth orbit with a typical orbiting period of 5400 seconds [3]. Used in such a space structure is, say, a one-inch thick graphite-epoxy composite, whose thermal diffusivity is taken approximately as $\alpha = 3 \times 10^{-6}$ ft²/sec [4]. With these numerical values, $\bar{\omega} = 2.7$ is obtained, thus establishing the range used in this analysis.

First, for the sake of demonstrating the methodology and procedure developed, the case of a 4-layer composite is considered. All layers are of equal thickness but have thermal conductivities in the ratios of 1, 2, 4, and 8, beginning with the inner layer. Their thermal diffusivities are taken to be equal. Figure 20 shows the calculated responses for the diffusion-cycle frequency $\bar{\omega}$ from 1 to 256. Finite slope changes are clearly indicated in Figure 20. A general conclusion from Figure 20 is

that at high frequencies, or at high harmonics of a low-frequency fluctuation, thermal effects are confined to a thin layer near the surface. The frequency-dependent nature of these distributions demonstrates the significance of the diffusivity-cycle parameter $\bar{\omega}$.

Computed values which made up Figure 20 are found to be most conveniently analyzed by the sequential method developed. If, instead, a direct analytical approach is used, the necessary algebra manipulations may become very prohibitive.

Results for 2-Layer Composites (Cyclic Surface Temperature)

Parallel to the computed results for the case of impulsive surface heating of two-layered composites, representative calculations for cyclic surface temperatures were made. The outer layer (coating) is taken to be 0.2 of the overall thickness. The first set of calculations is for reference only, with the outer layer identical to the inner. For the next set of calculations, the outer layer is assigned a larger thermal capacity ρC than the inner-layer value by a factor in order to ascertain the influence of thermal inertia of the outer shield. Subsequently, a third series of calculations was made with the outer layer having the same thermal inertia but with lower conductivities of 0.2 and 0.1 of the substrate layer. For all the computations cited, the diffusivity-cycle frequency $\bar{\omega}$ takes on the values of 1, 3, 6, 10 and 20, thus covering an expected span of variation.

Figure 21 shows the reference responses -- in reality for a single layer composite. The in-phase responses are indicated by the R-curves; and the out-of-phase responses, indicated by the I-curves, are 90° out

of phase of the cyclic surface temperature variations. The I-responses therefore represent travelling thermal waves or pulses. Formation of the complete responses is supplied by equation (67) or (69), which combines R and I together. Data in Figure 21 suggest a demarcation criterion of $\bar{\omega} = 1$. Below this value, the internal temperature variations are insignificant and the entire bulk may be treated as a single lump whose average temperature rises or falls in phase with the imposed surface temperature cycles. The out-of-phase waves are not insignificant to be ignored; for example, at $\bar{\omega} = 1$, the back surface temperature varies at 0.8 of the surface temperature excursion for the in-phase variation; however, the out-of-phase variation has a value of 0.4 of the surface cyclic magnitude. Interpreting these temperature responses in terms of the resulting thermal stresses, the near uniform distributions of the in-phase curves (R) indicate that the bulk stresses rise or fall with the surface temperature fluctuations but with only ± 10 per variances across the composite panels. Non-uniform temperature variations and the attendant thermal stress variations lead naturally to thermal moments and consequently bending or bowing of the panels. For the out-of-phase responses, the I-curves, there is a greater degree of non-uniformity of the temperature distribution, ranging from zero at the heating surface to -0.5 at the back surface. Hence, the thermal bending moments in the low-frequency cases may be due mainly to the shifted temperature responses.

As the surface temperature fluctuation goes above the critical value of $\bar{\omega} = 1$, the alternating temperature affect appears to be more confined in a thin surface layer, with the remainder of the panel less

affected. Hence, for high-frequency heating, damages, if any, are confined to the near surface region.

By taking the outer coat layer with 0.2 of the overall thickness and having a thermal capacity four times as large as the inner layer, the temperature responses were calculated and are shown in Figure 22. The effect of larger (pC)-values for the coat-layer is to have reservoir-like influence on the inner layer; the coat layer therefore alternately stores up the in-coming heat flux and gives out what has been stored before. In cyclic events, having a coat layer with a large thermal capacity is not very influential, as compared with its effect in impulsive heating analyzed previously where heat flow is not alternating. The data in Figure 22 demonstrate that although there is for both in-phase and out-of-phase a shift of the response curves towards the heating surface, the change is not materially significant from the curves in Figure 21 for a single-medium composite.

When, however, the outer layer has a lower thermal conductivity than the inner layer, thermal shielding thus afforded does substantially reduce the in-phase temperature fluctuation in the inner layer; but less so for the out-of-phase fluctuations. Data in Figures 23 and 24 demonstrate respectively these phenomena when the outer layer has a thermal conductivity equal to 0.2 and 0.1 of that of the inner layer. Particularly for high-frequency heating $\bar{\omega} = 3$ or above, the in-phase responses are nearly suppressed in the inner layer.

It is recalled that in the case of impulsive heat load when the heat flow direction is not alternating, low-conductivity thermal shields lead to very little change in the inner layer's temperature-time

history. For alternating heat flow, however, this type of shielding becomes particularly effective.

3.3 Cyclic Surface Heat Flux

Having obtained composite panel's responses to cyclic surface temperature variations, the analogous problem with periodic surface heat fluxes is a direct extension of the methodology established previously. Again, a Fourier series may be used to describe the surface heat flux of which a Fourier component may be represented by

$$q = q_A \cos \bar{\omega}\bar{\theta} + q_B \sin \bar{\omega}\bar{\theta} \quad (76)$$

Equation (76) is analogous to equation (54) for periodic surface temperature variations. The analytical developments are also parallel with the previous case, up to equation (57). However, the boundary condition at the heating surface is, instead of equation (59), given by

$$k_n (\partial T_n / \partial x) = q_A \cos \bar{\omega}\bar{\theta} + q_B \sin \bar{\omega}\bar{\theta} \quad (77)$$

Since the heat flux terms can be expressed by the following exponential terms

$$q = (q_A/2)(e^{i\bar{\omega}\bar{\theta}} + e^{-i\bar{\omega}\bar{\theta}}) - (iq_B/2)(e^{i\bar{\omega}\bar{\theta}} - e^{-i\bar{\omega}\bar{\theta}}) \quad (78)$$

the complete solution is made of individual solutions, each satisfying an individual heat flux component term in equation (78). To obtain the individual solutions, a non-dimensional temperature is defined by

$$\bar{T}_A = (k_1 T_A / L_n q_A) \quad (79)$$

where k_1 is the thermal conductivity of the first layer, L_n is the total thickness, and q_A is the heat flux Fourier coefficient. For the first term of the four in equation (78), the solution (A-Solution) is assumed to have the following form for the j -th layer in the composite:

$$\bar{T}_{A-j} = (1/2)e^{-i\bar{\omega}\bar{\theta}} e^{\beta_j \bar{x}} \quad (80)$$

The exponent, β_j is defined by equation (61). For the first layer, the solution, analogous to equation (62), is expressed by

$$\bar{T}_{A-1} = (1/2)e^{i\bar{\omega}\bar{\theta}} \left[G_1 \cosh \beta_1 \bar{x} \right] \quad (81)$$

and, for other layers, by

$$\bar{T}_{A-j} = (1/2)e^{i\bar{\omega}\bar{\theta}} \left[G_j \cosh \beta_j (\bar{x} - \bar{L}_{j-1}) + H_j \sinh \beta_j (\bar{x} - \bar{L}_{j-1}) \right] \quad (82)$$

At the heating surface, $\bar{x} = 1$, the heat flux is to satisfy the first term of equation (71); and by using equation (75), the boundary condition becomes

$$\beta_n G_1 (k_n / k_1) \left[(G_n / G_1) \sinh \beta_n (1 - \bar{L}_{n-1}) + (H_n / G_1) \cosh \beta_n (1 - \bar{L}_{n-1}) \right] = 1 \quad (83)$$

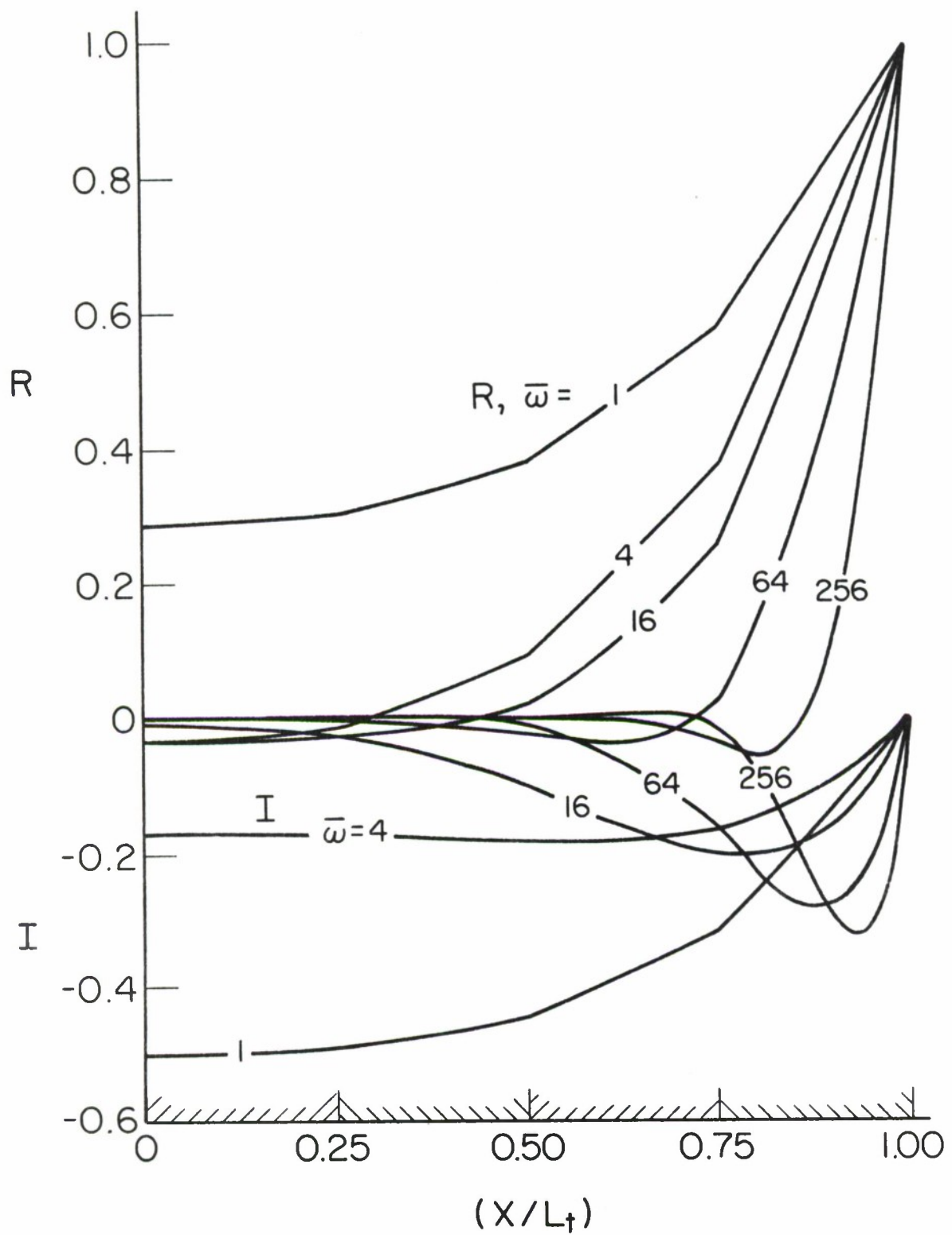


Figure 20. Temperature Functions of a 4-Layered Composite Due to Periodic Surface Temperature Variation

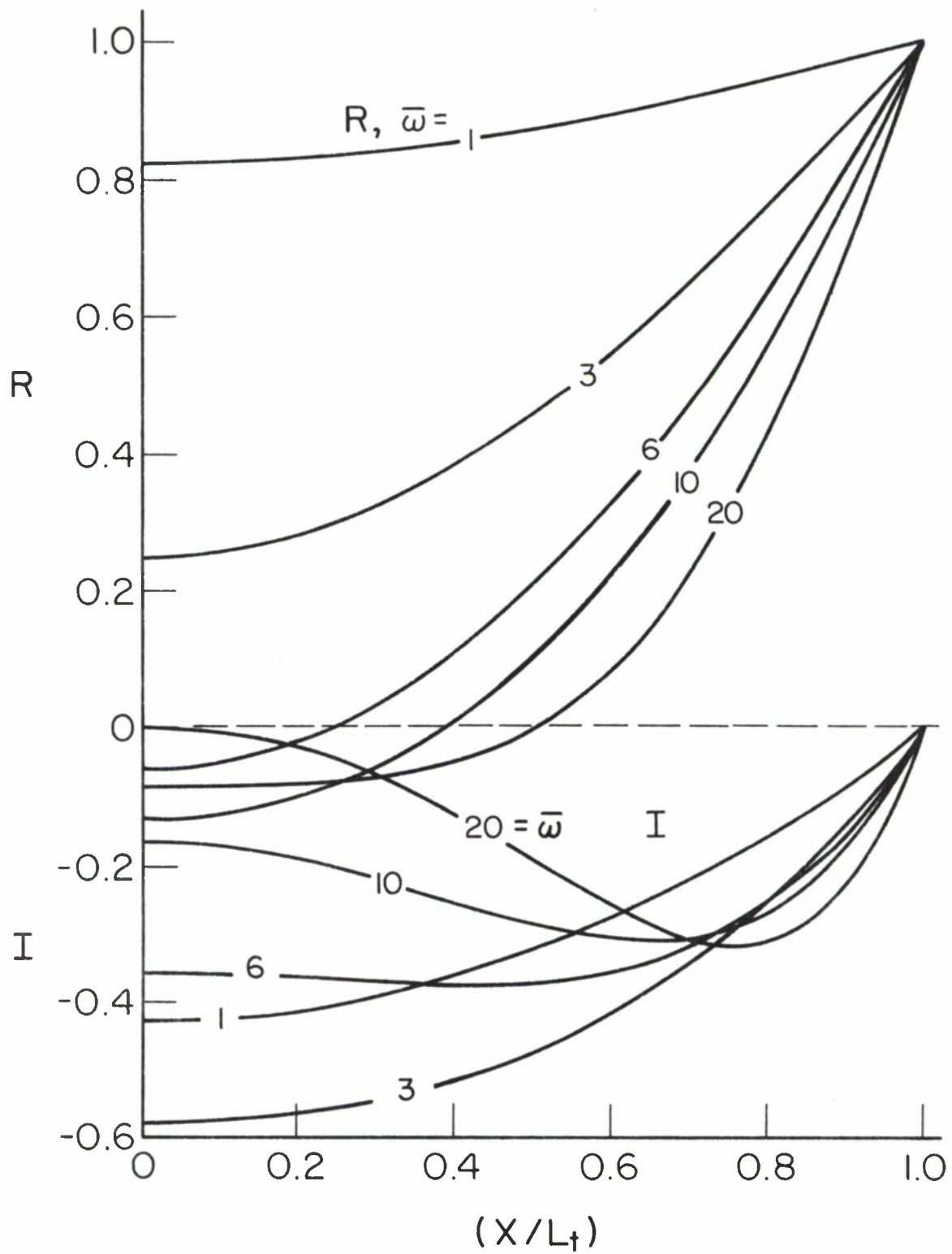


Figure 21. Temperature Responses of a Single-Layer Composite by Periodic Surface Temperature Variation

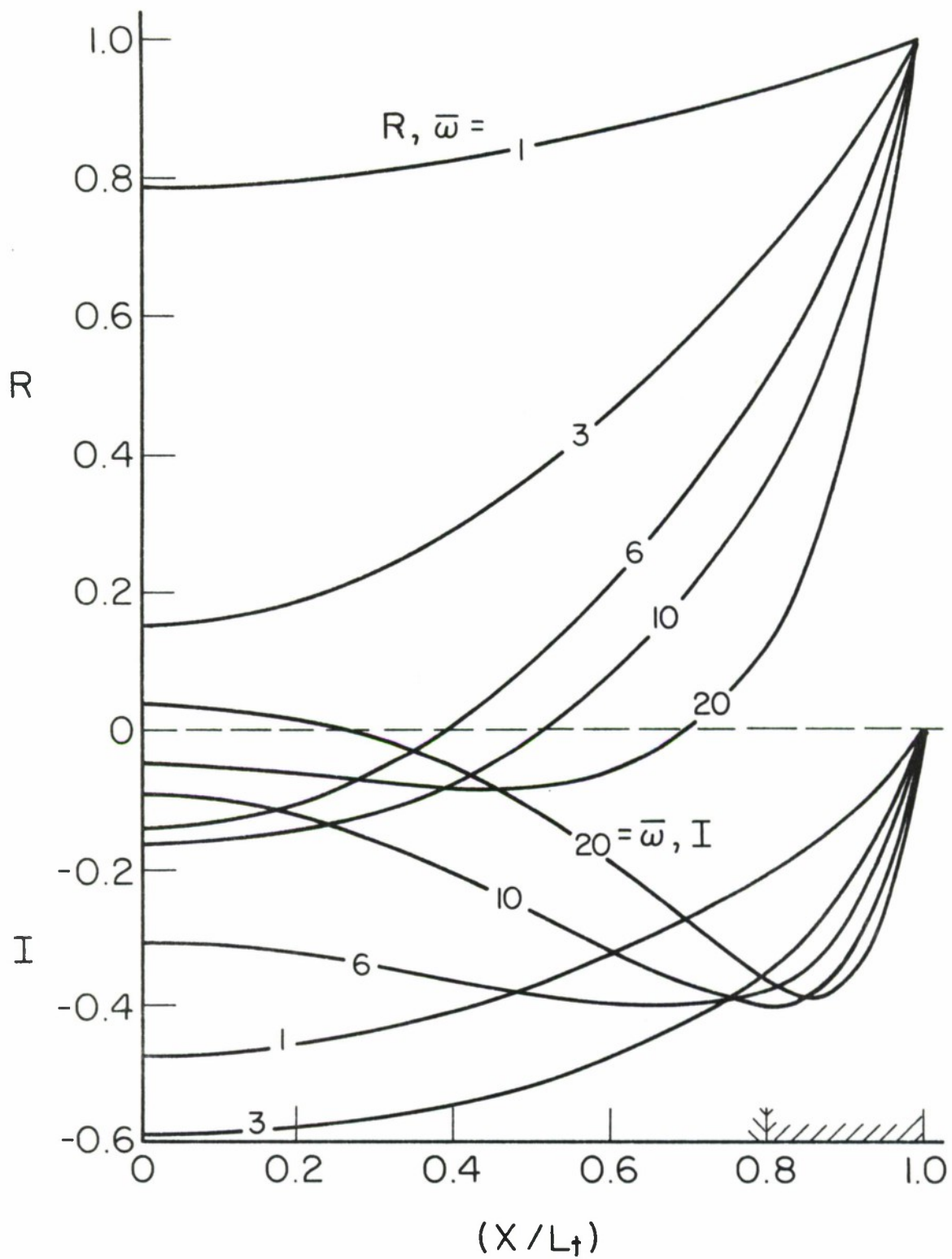


Figure 22. Temperature Responses of a Two-Layer Composite by Periodic Surface Temperature Variation, $(\rho C)_c / (\rho C)_s = 4$

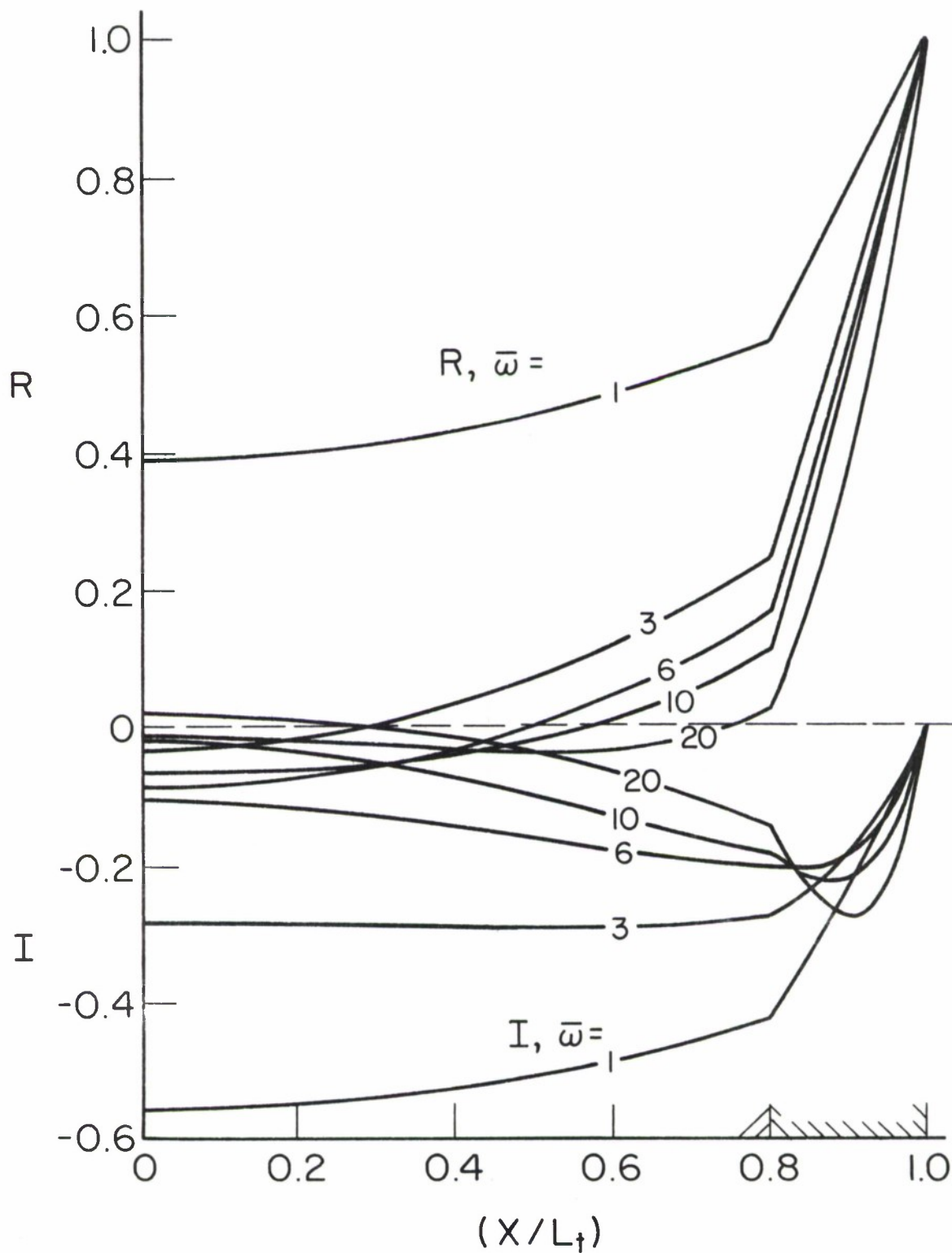


Figure 23. Temperature Responses of a Two-Layer Composite by Periodic Surface Variation, $k_c/k_s = 0.2$

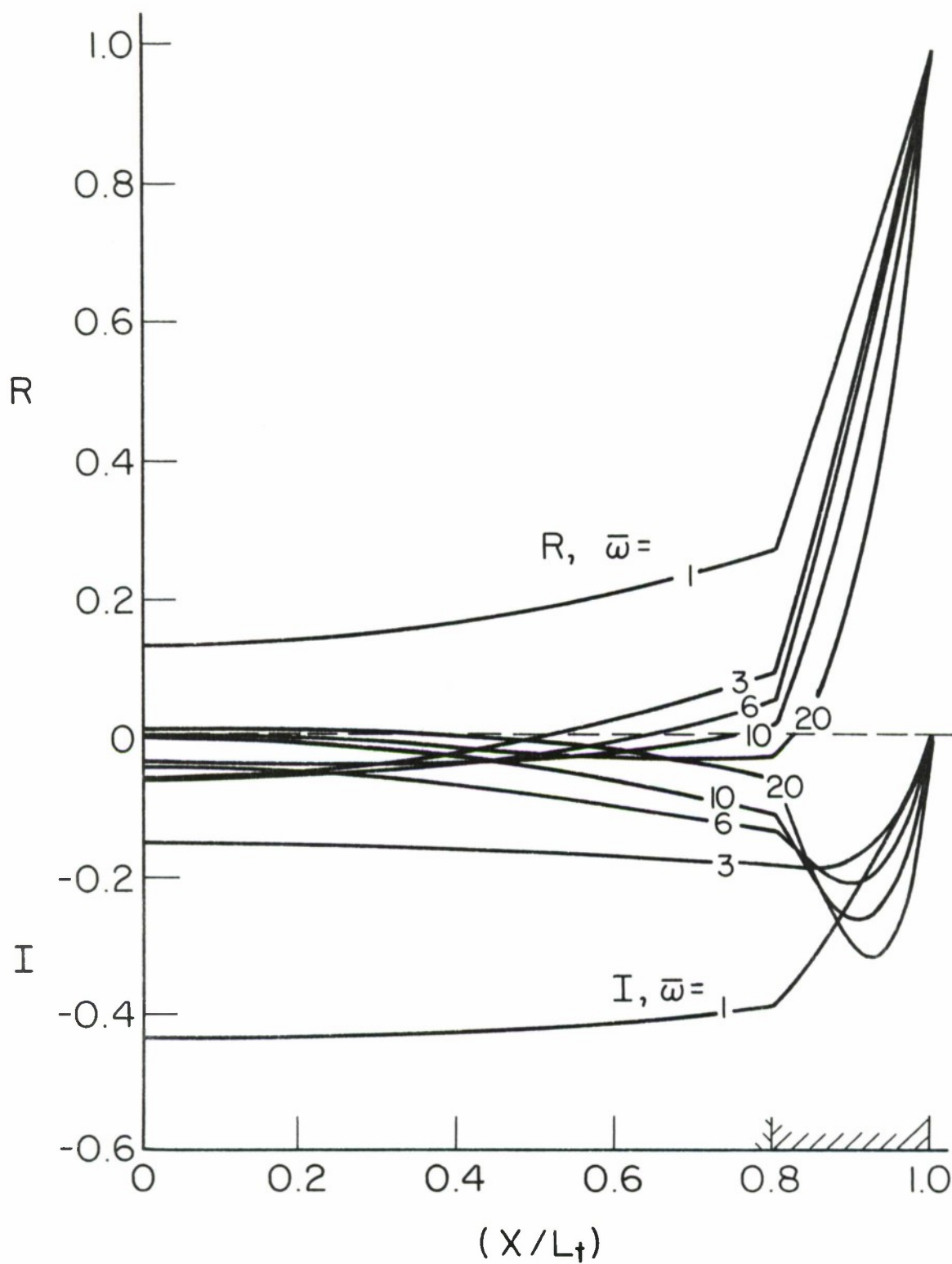


Figure 24. Temperature Responses of a Two-Layer Composite by Periodic Surface Temperature Variation, $k_c/k_s = 0.1$

The procedure of obtaining the coefficients G's and H's is identical to that used previously for the problem with a specified surface temperature fluctuation. Equation (83) is used to obtain G_1 , instead of equation (65).

With the A-solution thus obtained -- defined by equations (81) through (83) -- which satisfies the heat flux boundary condition described by the first of the four terms on the right of equation (78), the complete solution for the surface heat flux $q_A \cos \omega \theta$ can be constructed by a procedure similar to that for the cyclic surface temperature case, treated in 3.2.

To be more specific, the real and imaginary parts of the terms inside the brackets of equation (82) are expressed by the following:

$$\begin{aligned} G_j \cosh \beta_j (\bar{x} - \bar{L}_{j-1}) + H_j \sinh \beta_j (\bar{x} - \bar{L}_{j-1}) \\ = R_j + iI_j \end{aligned} \quad (84)$$

Then the complete temperature response to the surface heat flux fluctuation of $q_A \cos \omega \theta$ is given by

$$\bar{T}_{A-j} = (k_1 T_{A-j} / L_n q_A) = R_j \cos \bar{\omega} \bar{\theta} - I_j \sin \bar{\omega} \bar{\theta} \quad (85)$$

Similarly, the complete temperature response to the surface flux $q_B \sin \omega \theta$ is

$$\bar{T}_{B-j} = (k_1 T_{B-j} / L_n q_B) = R_j \sin \bar{\omega} \bar{\theta} + I_j \cos \bar{\omega} \bar{\theta} \quad (86)$$

In both equations (85) and (86), the layer index j varies from 1 through

n. An apparent structure of the solution is that R_j is the in-phase (with heat flux) part and I_j the out-of-phase part.

Low Frequency Analysis. Before discussing numerical results it is important to point out that the out-of-phase response I_j is where heat storage occurs and the in-phase response R_j is that profile through which heat conduction occurs. To demonstrate this fact, consider a single-layer composite. The response to $q_A \cos \omega \theta$ is the following:

$$\bar{T}_{A-1} = (k_1 T_{A-1} / L_1 q_A) = R_1 \cos \bar{\omega} \bar{\theta} - I_1 \sin \bar{\omega} \bar{\theta} \quad (87)$$

where R_1 and I_1 are derived from equation (81) and are expressed by

$$R_1 + i I_1 = \cosh \beta_1 \bar{x} / \left[\beta_1 \sinh \beta_1 \right] \quad (88)$$

The complex coefficient β_1 is $(1+i)\sqrt{\bar{\omega}/2}$. The respective roles played by R_1 and I_1 in equation (87) can be made clear by referring to the diffusion equation (57) for the layer. Integrating the diffusion equation from $\bar{x} = 0$ to $\bar{x} = 1$, where a prescribed heat flux of $q_A \cos \omega \theta$ occurs and using equation (87) for the temperature response, the integrated form becomes

$$\frac{d}{d\bar{\theta}} \left[\cos \bar{\omega} \bar{\theta} \int_0^1 R_1 d\bar{x} - \sin \bar{\omega} \bar{\theta} \int_0^1 I_1 d\bar{x} \right] = \cos \bar{\omega} \bar{\theta} \quad (89)$$

The right-hand side of equation (89) is the surface heat flux term; thus equation (89) shows that heat flux is accumulated in the I_1 -term and

correspondingly the boundary condition of heat flux at $\bar{x} = 1$ is satisfied via the R_1 -term.

Because of the above examination of the terms' composition, it is of importance to note that if the cyclic heat flux condition is such that heating or cooling takes place over a long period of time, i.e., $\omega \rightarrow 0$ or $\beta \rightarrow 0$, then the heat accumulation terms I 's tend to be large since there is more time to pile up. To substantiate that, the one-term solution of equation (88) can be decomposed into its real and imaginary parts: Since β is a complex constant, asymptotically small values of β or ω lead to the following series expansion in terms of ω as the parameter:

$$\frac{\cosh \beta \bar{x}}{\beta \sinh \beta} = \left(\frac{\bar{x}^2}{2} - \frac{1}{6} \right) - i (1/\bar{\omega}) + \dots \quad (90)$$

Thus the imaginary part I , is inversely proportional to ω or directly to the cyclic period, a clear indication of the heat accumulation effect. Moreover, for quasi-steady state heating or cooling, i.e., $\omega \rightarrow 0$ the real part R , becomes asymptotically parabolic, as indicated by the leading term of equation (90).

It is clear that for any combination of the physical parameters, whether it is a single-layer or multi-layer composite, there invariably exist asymptotic distributions of the in-phase and out-of-phase parts, R and I for different layers. Their mathematical representations may be more involved, but the existence can be easily established.

Numerical Results for 2-Layer Composites (Cyclic Flux). As a reference combination, consideration is given to a two-layer composite

with both layers having identical physical properties. In essence, it is a single layer analysis. Computed response functions R and I are presented in Figure 25 for diffusion-cycle frequencies of $\bar{\omega} = 1, 6, 10$ and 20.

It is clear from the graphical display that for $\bar{\theta} = 1$, the distribution of I is almost asymptotic, which is given by equation (90) as -1 . A slight variation from $\bar{x} = 0$ to $\bar{x} = 1$ is, however, noted, indicating its dependency on $\bar{\omega}$ yet. For the real part, the distribution for $\bar{\omega} = 1$ is almost indistinguishable from that in equation (90) for $\bar{\omega} \approx 0$. Translating these observations into thermal stress considerations, it is the bulk temperature rise that yields thermal stresses. Hence it is the I -distribution that governs the stress magnitudes; and at low frequencies there would be higher stresses. The thermal stresses caused by the R -distributions are, however, in self-equilibrium and these stresses contribute a thermal moment across the composite slab, resulting in its flexural bending as a consequence. Naturally, as the frequency increases, the temperature distribution functions R and I diminish in magnitude and so do the thermal stresses. These qualitative trends also apply to multi-layer composites.

With two-layer composites, numerical computations were completed first with the outer layer (0.25 of the inner layer thickness) having a larger thermal capacity of 4 times the inner value. The external coating behaves as a thermal sink with respect to the surface heating and results in a general reduction of the temperature responses in the inner layer. Figure 26 indicates the response curves for R and I in the same frequency range as in Figure 25. While the real part R (in-phase with surface flux) shows very little change from those in Figure 25, the

imaginary part I (out-of-phase and for heat storage) indicates significant reductions in magnitude, thus reflecting the influence of the thermal capacity in the outer layer.

The other parameter of interest is the thermal conductivity. By decreasing the coat layer conductivity to 0.2 of the inner layer (with equal thermal capacity for both), the response curves are shown in Figure 27. A notable feature is that the I-distributions are very much similar to those in Figure 25, indicating little effect of low conductivities of the coat layer on the level of the bulk temperature change. There are, however, considerable increases of the R-distributions over those of Figure 25 for single layer performances. With the outer layer acting as a heat barrier, temperature differentials across the barrier are increased to account for the specified surface heat flux. Hence from a thermal protection viewpoint, low conductivity in the outer layer tends to produce greater thermal stresses.

4. CONCLUSIONS

In this report, two transient heat conduction problems for application to the thermal evaluation of composite materials are analyzed and discussed.

The purposes of these two analyses are at least two-fold: One is to demonstrate by detailed numerical results that composite materials with a larger in-plane thermal conductivity than the transverse value exhibit lower surface temperatures when the thermal loading consists of irradiation by a concentrated cylindrical beam. Effective radial heat spread along the in-plane direction serves to reduce local heat

accumulation and thereby mitigates heat-spot temperature rises. Accordingly, preventing or delaying damage due to high-intensity thermal radiation on composite surfaces can be enhanced by using materials with large in-plane thermal conductivities. The second objective of the investigation is to develop a methodology whereby composite panels undergoing cyclic heating and cooling can be analyzed for their periodic temperature responses. This is particularly important for determining thermal stresses resulting from alternating temperature fluctuations. The methodology developed is especially useful since numerical approaches can be very time-consuming and unreliable.

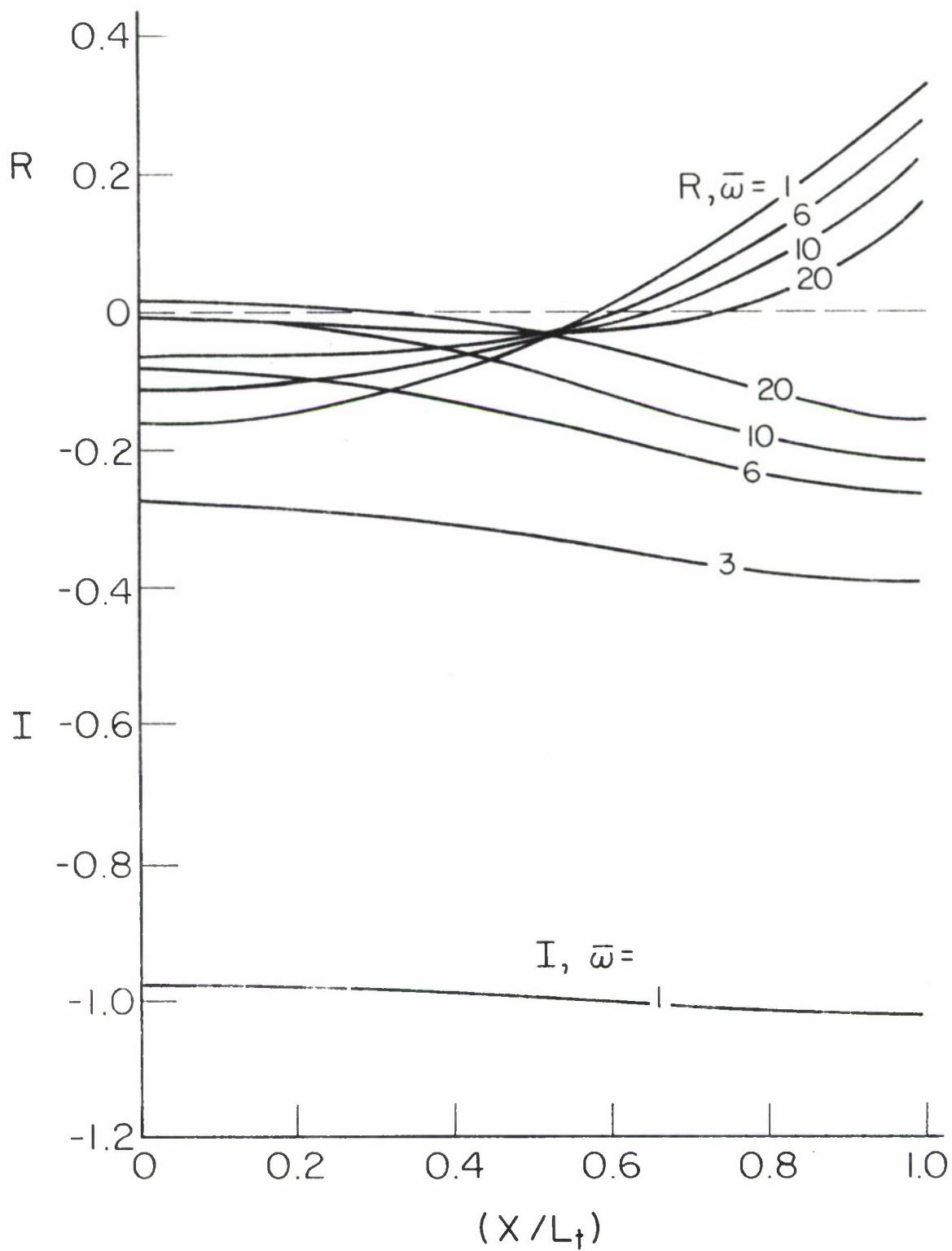


Figure 25. Temperature Responses of a Single-Layer Composite by Periodic Surface Heat Flux

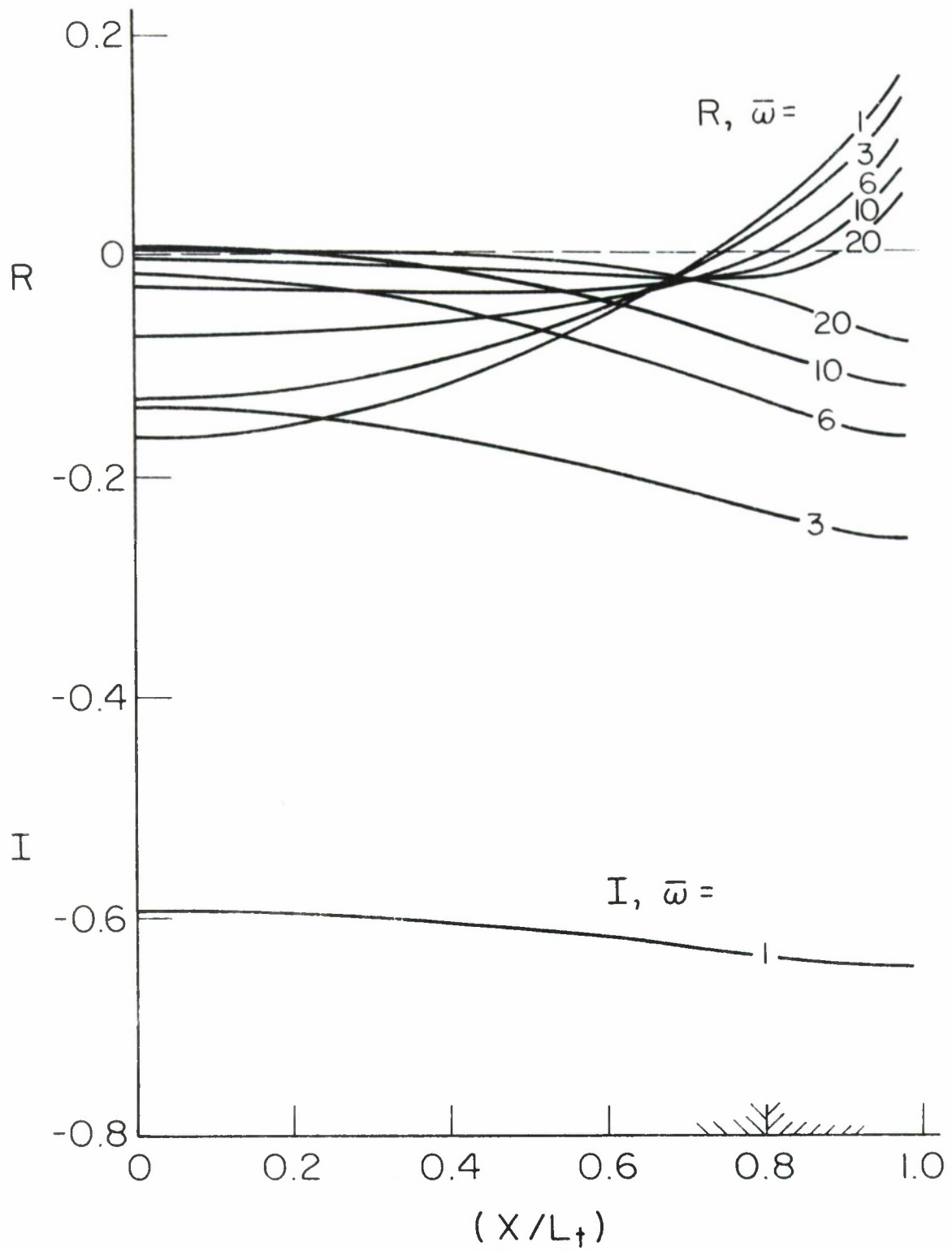


Figure 26. Influence of Large Coating Layer Thermal Capacity on Temperature Responses of a Two-Layer Composite by Periodic Surface Heat Flux

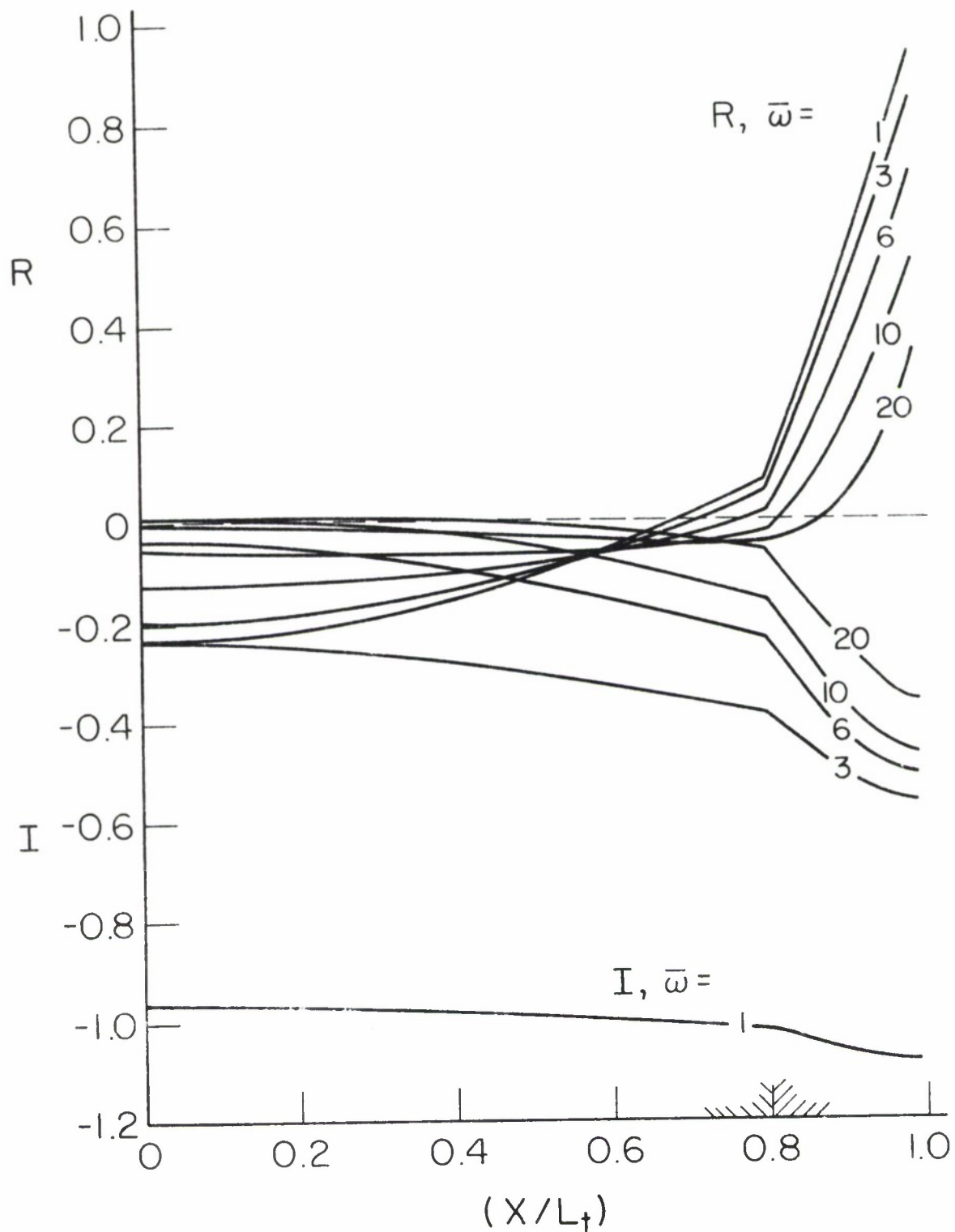


Figure 27. Influence of Low Coating Layer Thermal Conductivity on Temperature Responses of a Two-Layer Composite by Periodic Surface Heat Flux

REFERENCES

1. Roache, P.J., Computational Fluid Dynamics, Hermosa Publishers, 1976, pp. 95-99.
2. Carslaw, H.S., and Jaeger, J.C., Conduction of Heat in Solids, Oxford: Clarendon Press, 1947.
3. Thorton, E.A., and Paul, D.B., "Thermal-Structural Analysis of Large Space Structures," AIAA Paper No. 83-1018, to be published in AIAA Journal.
4. Pan, L. and Boyee, W.F., "Thermal Conductivities and Diffusivities of Graphite-Epoxy Composites," AFWAL-TR-83-3002, Feb., 1983.

NOMENCLATURE

a	heat beam radius
C	specific heat
i,j	node indexes
k	thermal conductivity
L	layer thickness
P	period of fluctuation
Q,q	heat flux intensity
q_A, q_B	Fourier coefficients for heat flux
r	radial coordinate from spot (beam) axis
T	temperature rise
w	panel thickness
x	depth coordinate from insulated surface
z	depth coordinate from heating surface
R	real part of a complex function
I	imaginary part of a complex function

Non-dimensional Variables

$$\bar{z} = (z/a)$$

$$\bar{r} = (r/a) \, k_r/k_z$$

$$\bar{\theta} = (\alpha_z \theta/a^2) \quad \text{or} \quad (\alpha_s \theta/L_t^2)$$

$$\bar{T} = (k_z T/aQ)$$

Greek Symbols

Δ	grid size $\Delta = \Delta \bar{r} = \Delta \bar{x} = \Delta \bar{z}$
δ	nondimensional time step
α	thermal diffusivity $k/\rho C$
ρ	density
ω	circular frequency
β	frequency parameter

Subscripts

b	back surface, beam center
c	coating layer
j	ordinal number for layer
o	beam spot center
r	radial direction
s	substrate layer
t	total
z	depth direction

APPENDIX

Comparison of Results with Different Grid Sizes

It is well established that computational results based on the finite-difference approach are sensitive to the grid size used. The finer the grid size, the more accurate are the results; but far more time-consuming is the task. Halving the grid size usually increases the process time by a factor of eight and more. For this reason, some balance is needed between accuracy and excessive computational effort.

In the computational effort undertaken in this report, the grid size is obtained by dividing the non-dimensional heat spot radius into five divisions. Since the non-dimensional radius is defined by $\bar{r} = (r/a)\sqrt{k_z/k_r}$ where a is the beam radius, each division of \bar{r} is therefore equal to $(\sqrt{k_z/k_r})/5$. In the depth direction, the dimensionless variable is $\bar{z} = (z/a)$, each step $\Delta\bar{z}$ is made equal to $\Delta\bar{r}$, and the number of divisions is determined by the width w and the ratio of k_z/k_r . In this way, a grid uniform in the non-dimensional coordinates, but non-uniform in the physical coordinates, is achieved.

In order to ascertain typical differences in the results due to different grid sizes, the case of $k_z/k_r = 1$ and $w/a = 1$ was analyzed by two parallel computations: one using 5 divisions and the other, 10 divisions for the heat spot radius. Results of these two comparative calculations are presented in Figure A-1, which shows the spot center temperature rises as heating proceeds. Naturally, the results based on 10 divisions for the heat spot are more reliable than those based on a coarser grid. However, the difference in the temperatures at the end of

the non-dimensional time $\bar{\theta} = (\alpha_z \theta / a^2) = 4$ is quite small compared to their mean value: the difference being 0.05 out of their average value of 1.2 at the spot center. At the back surface of the slab, opposite to the spot center, the difference becomes 0.07 out of their mean value of 0.9. The computer process times were 4 seconds and 55 seconds respectively. For other conductivity ratios $k_z/k_r < 1$ with a much finer grid in the z-direction than in the r-direction, the computer process time was found to be much more than 55 seconds.

Additional comparisons of these two parallel sets of results are presented in Figures A-2 and A-3. The former shows, at the end of heating time $\bar{\theta} = 10$, the isothermal lines of temperature 0.8, 0.6 and 0.4 of the spot center temperature. The results using different grid sizes are nearly coincidental to each other. Thus, the use of a smaller number of division is deemed adequate. Shown in Figure A-3 are the temperature profiles in the r-direction on the front and back surface at $\bar{\theta} = 10$. Even though the spot-center temperature rises are 1.49 and 1.41 for 5 and 10-direction calculations, their normalized (with respect to the spot-center temperature) curves are parallel to each other. Thus, the use of 5-division appears quite adequate for the demonstrative analysis presented in this report.

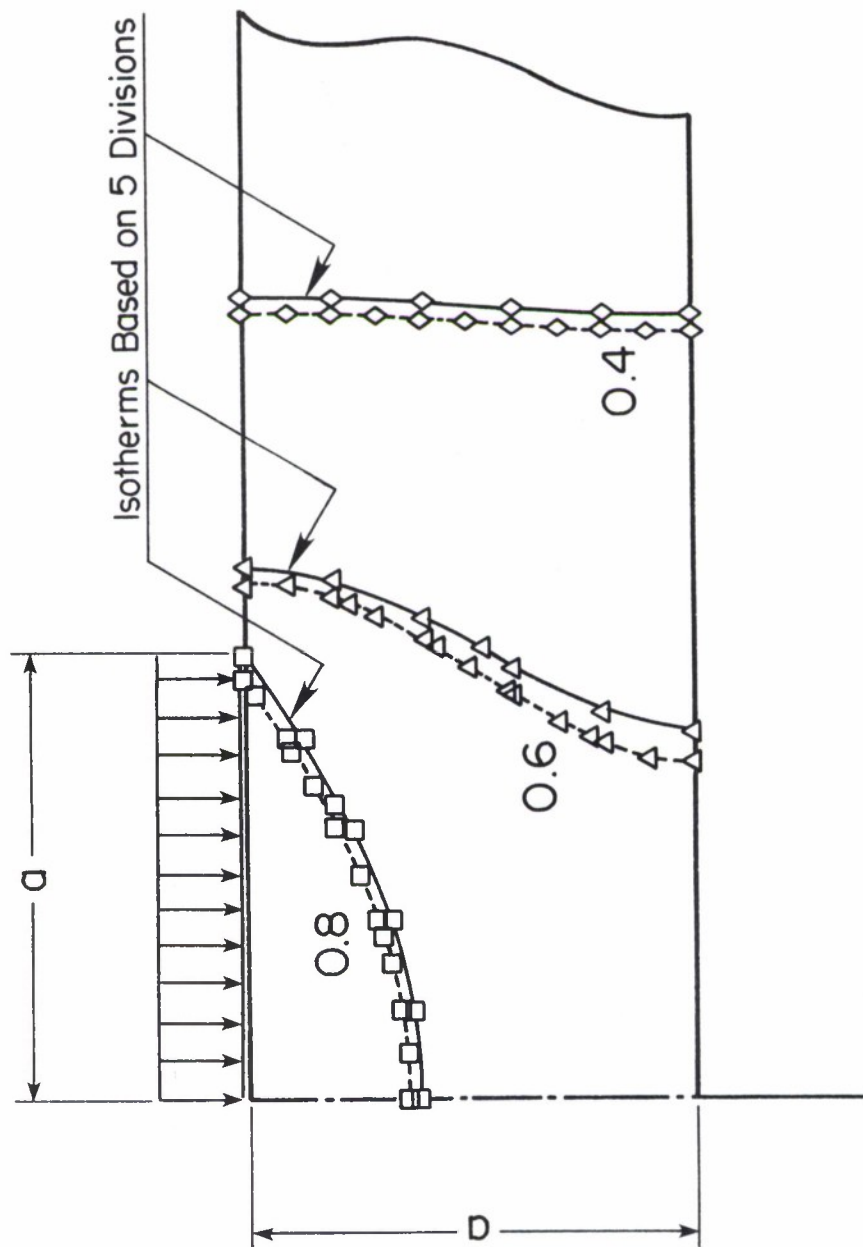


Figure A-1. Effect of Grid Size on Temperature Calculations, Spot Heating

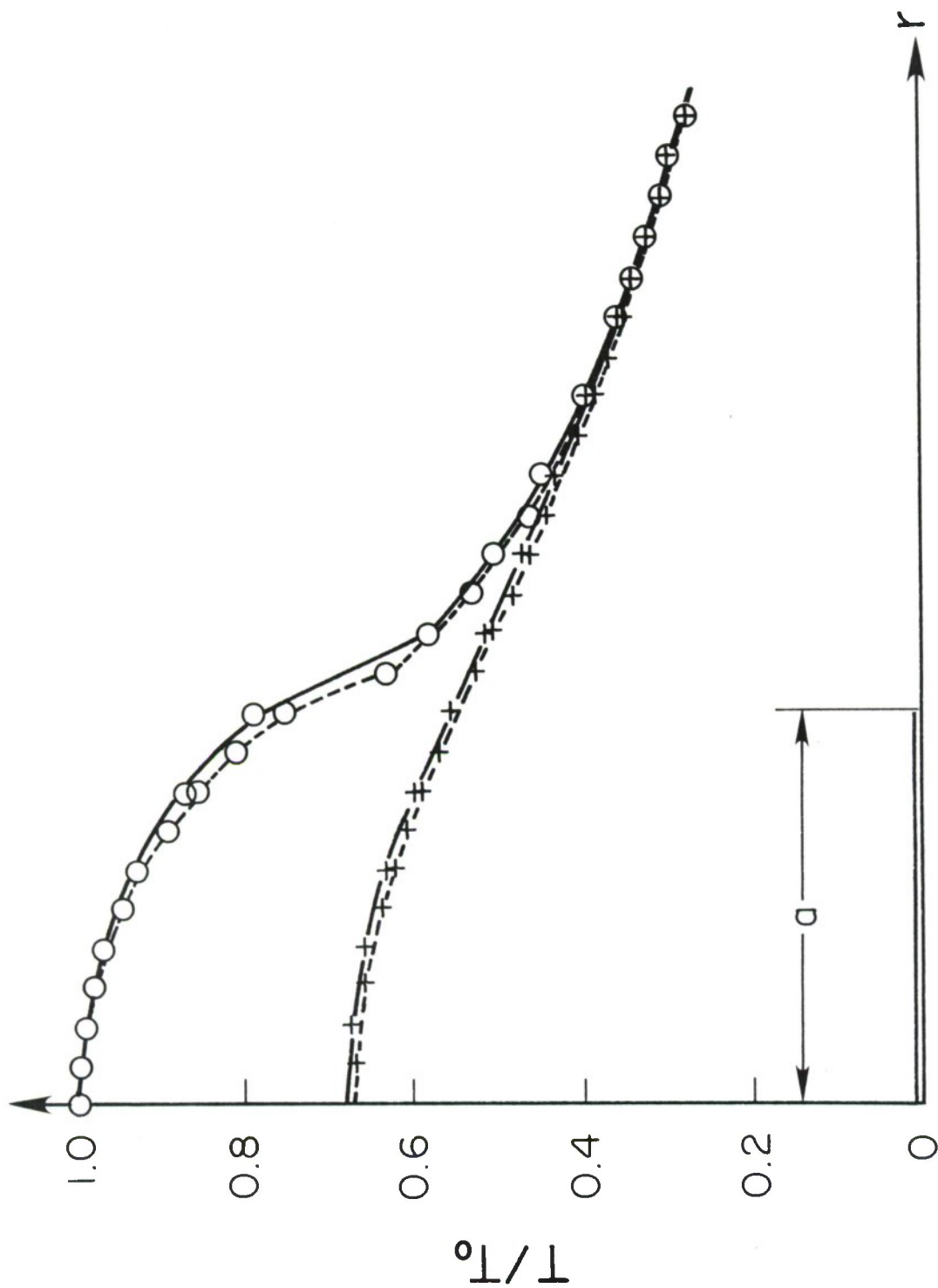


Figure A-2. Effect of Grid Size on Isothermal Contours, Spot Heating

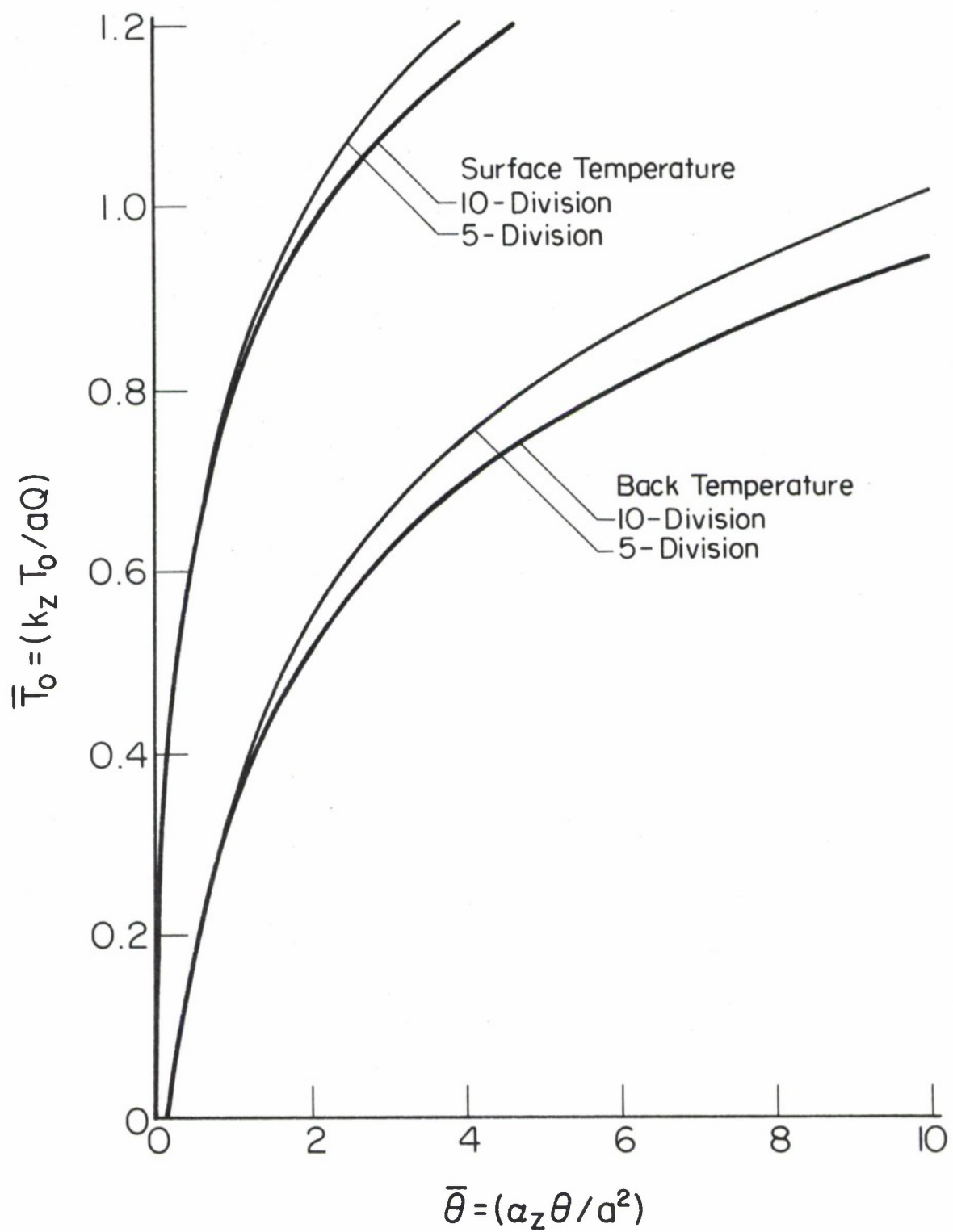


Figure A-3. Effect of Grid Size on Surface Temperature Profiles, Spot Heating